JET FRAGMENTATION VIA RECOMBINATION OF PARTON SHOWERS AND ITS MEDIUM MODIFICATION IN HEAVY ION COLLISIONS

A Dissertation

by

KYONG CHOL HAN

Submitted to the Office of Graduate and Professional Studies of
Texas A&M University
in partial fulfillment of the requirements for the degree of

DOCTOR OF PHILOSOPHY

Chair of Committee,	Che-Ming Ko
Committee Members,	Rainer J Fries
	Carl A. Gagliardi
	Sherry J Yennello
Head of Department,	George R. Welch

May 2016

Major Subject: Physics

ABSTRACT

For jets produced in relativistic heavy ion collisions, the presence of the quark-gluon plasma (QGP) formed in the collisions not only affects their energies but is also expected to affect their hadronization. In this dissertation, we have studied the influence of the QGP on jets by treating the jet as shower partons, which are then converted to hadrons via their recombination among themselves as well as with the thermal partons in the quark-gluon plasma. To verify the feasibility of treating the hadronization of energetic jets by recombination of shower partons, we have computed hadron spectra in $e^+ + e^-$ collisions. Including contributions from resonance decays and from the string fragmentation of the remnant partons left after the recombination by using a subroutine of PYTHIA, we have found that the resulting spectra of longitudinal momentum fractions and transverse momenta for pion, kaon, nucleon, and Λ reproduce reasonably those from the string fragmentation obtained in PYTHIA. The medium effect on the conversion of jets to hadrons is then studied for heavy ion collisions at both RHIC and LHC by using the blast-wave model for generating the thermal partons in the QGP. In obtaining the shower partons from jets, we have included their energy loss due to interactions with thermal partons in QGP. We have found that including hadron production from the recombination of shower partons with thermal partons leads to a significant enhancement in the production of hadrons with intermediate transverse momenta at both RHIC and LHC. Our results show that the recombination model can reproduce well the experimental measurements conducted at both RHIC and LHC, thus suggesting the importance of medium modifications in the conversion of jets to hadrons in the presence of a QGP.

DEDICATION

To the memories of Yongha Han (1943-2000?), my father, and Jun-gil Shin (1944-1996), my old teacher.

ACKNOWLEDGEMENTS

First of all, I earnestly thank my dissertation advisor, Prof. Che-Ming Ko. He accepted me as his student at Texas A&M University and taught me many things during my PhD years. Without his patience, guidance, and untiring dedication, I would never have completed this dissertation. I am grateful to Prof. Rainer Fries. As a convener of our Recombination Group in the JET Collaboration, he allowed me to work for this project. He gave me insightful comments and suggestions when I had troubles in my research and taught me kindly when I asked questions in my studies. I would like to thank two other members of my dissertation committee - Prof. Carl Gagliardi and Prof. Sherry Yennello - for giving me useful comments and feedbacks during my final defense presentation. I also thank Prof. Ralf Rapp for sitting in my final defense presentation and giving me constructive comments.

I am thankful to the JET Collaboration members: Prof. Xin-Nian Wang, Prof. Abhijit Majumder, Prof. Steffen Bass, Dr. Shanshan Cao, and Prof. Ulrich Heinz for giving us helpful comments in the meetings and sending us sample data for testing our recombination code.

I would particularly like to thank Prof. Su Houng Lee and Prof. Sungtae Cho for reading carefully a draft of this dissertation and suggesting me several corrections.

I want to thank all members of the Cyclotron Institute at Texas A&M University for providing me wonderful environment for my research.

I would like to express my gratitude to my current and former colleagues in the Prof. Ko's Nuclear Theory Group - Feng Li, Yifeng Sun, Dr. Taesoo Song, Prof. Jun Xu, Prof. Yunpeng Liu, and Prof. Hanzhong Zhang - for giving me many helps during my research.

I owe my deepest gratitude to Rev. John Reasons, a senior pastor at the A&M United Methodist Church, and members of the "*Open Door*" Sunday School class for supporting me and praying for me and my family. Special thanks Dr. Ken Lee and Mrs. Susan Lee for reading Chapter 1 of my draft and checking English grammar and expressions.

I would like to show my gratitude to North Korean defector friends and friends loving North Korean defectors - Rev. Steve Jung, Dr. Aeran Lee, Mr. Il-Joo Kim, Rev. Myunghee Uhm, Lisa Orme and Dr. Terry Orme, Julian Joseph, Henry Song, Jinseo Lee, and Juha Baek - for supporting me.

This work would have not been possible without the support of the DOE Grant No. DE-FG02-10ER41682: thank you to Xin-Nian Wang as a project director. I gratefully acknowledge financial supports from the following organizations and private donors: Oak Han Heum Scholarship Foundation at SaRang Community Church, North Korean Refugees' Foundation, Young-Bin Min, the CEO of YBM Inc., and Sunshik Min, the President of YBM Inc., Mr. Im Sik Kim, Korean American Scholarship Foundation, and the National Unification Advisory Council.

My heartfelt appreciation goes to my parents-in-law and sisters-in-law for their supports and prayers.

I also thank my mom, my sister, and my brother in South Korea for their unconditional supports and prayers of tears.

I owe debt of gratitude to my wife, Wonok Lee, for supporting me throughout this challenging time in my life and rasing my children. I also thank to David and Jason, my two sons and my biggest fans, for cheering me and giving the sustenance to my life every day.

Today, I miss so much my father, Yongha Han (1943-2000?), who had supported me and passed away alone in North Korea, and my old teacher, Jun-gil Shin (1944-

1996), who led me to physicist's journey when I was a middle school student. I would like to dedicate this dissertation to the memories of them.

TABLE OF CONTENTS

Page

LIST OF FIGURES

FIGURE Page

LIST OF TABLES

TABLE Page

1. INTRODUCTION

Matter is made up of molecules that consist of atoms. Atoms are made up of a nucleus and one or more electrons. Electrons are believed to be unsplittable. On the other hand, nuclei are composed of protons and neutrons. In general, protons and neutrons are bound states of quarks and gluons. There are gluons mediating forces between quarks. It was believed that quarks and gluons could not exist on their own, and they were always confined inside hadrons, which are bound states of quarks. However, the quark-gluon plasma (QGP) or quark soup, in which quarks, antiquarks, and gluons with restored chiral symmetry are deconfined and they roam freely, can exist at extremely high temperature and/or high density. This state of quark matter existed in the Early Universe after the "Big Bang". To reproduce this extreme state of matter, particle accelerators such as the Relativistic Heavy Ion Collider (RHIC) at the Brookhaven National Lab (BNL) and the Large Hadron Collider (LHC) at the European Organization for Nuclear Research (CERN) were built to collide nuclei at extremely high energies.

In relativistic heavy ion collisions carried out at RHIC and LHC, the QGP consisting of unbound quarks and gluon can be created. However, colored quarks and gluons in QGP are soon (a few fm/c) bound into colorless hadrons as the QGP expands and cools, as a result of the color confinement or absence of isolated color charges. Thus, only hadrons can be measured in experiments. In studying the properties of produced QGP, it is important to understand how quarks and gluons form the hadrons that are observed in the final state. This also applies to quarks and gluons that are produced in initial hard collisions between incident nucleons. The last process is called *hadronization*. When quarks and gluons bind to form hadrons,

their interactions become strong, so the perturbation theory is not applicable for describing the hadronization. Since the hadronization of quarks and gluons is a non-perturbative process, it has often been described by phenomenological models. A similar situation exists in elementary collisions at high energies, where the initially produced jet partons (quarks and gluons) from hard collisions, which can be described by the perturbative QCD, are converted to hadrons by the fragmentation functions that are fitted to experimentally measured hadron spectra. The independence of the fragmentation process from the initial hard process [12, 13] reflects the factorization theorem in QCD that perturbatively calculable short-distance cross sections for the hard scattering and long-distance fragmentation functions for the hadronization can be treated separately. In relativistic heavy ion collisions, it has been found, however, that the fragmentation of energetic jets produced from initial hard collisions cannot describe the measured hadron spectra at the intermediate transverse momentum region, which, on the other hand, is well described by the parton recombination or coalescence model [11, 14, 15, 16].

In this dissertation, the parton recombination model is extended to describe the jet fragmentation function by the recombination of parton showers inside jets. Moreover, we have studied the medium modification of jet fragmentation by including the recombination of shower partons in jets with thermal partons in QGP. Since jets lose energy while traversing through a medium, we have used quenched jets after their interactions with the medium [17, 18]. For shower partons in jets, they are obtained from the PYTHIA program, which is a Monte Carlo generator for elementary collisions at high energies. Since only the energy-momentum information of shower partons are provided by PYTHIA, we have determined the space-time information of shower partons by taking the lifetime of each parton in its rest frame to be the inverse of its virtuality. Using the resulting phase-space information of shower partons, we

have studied hadron production from a jet by the recombination of shower partons and compared the results with those obtained using the empirical jet fragmentation functions. To study the medium effect on hadron production from jet fragmentation, we have allowed shower partons in jets to also recombine with thermal partons in QGP. For the thermal partons, they are obtained from a blast wave model. To take into account the energy loss of jets in QGP [19, 20, 21], we have used the energy loss formula in Ref. [21] to the leading jet during each step of its branching into shower partons. We have then calculated the hadron spectra by including contributions from recombinations of thermal partons among themselves, thermal partons with shower partons, and shower partons among themselves. The resulting hadron spectra reproduced very well the experimental data from RHIC and LHC. Since our results show that the contribution of thermal-shower recombination enhances significantly the hadron spectra at intermediate momenta, studying these hadrons thus provide the possibility to investigate the medium effect of jet fragmentation as well as the properties of the QGP.

This dissertation is organized as follows: In Section 2, we review several models for hadronization of partons. In Section 3, we describe how parton showers produced from hard scattering are generated by a Monte Carlo event generator, which will be used in the next Section. We then demonstrate in Section 4 how jet fragmentation in the vacuum is reproduced by the recombination of shower partons. A part of this section is published in Physical Review C [3]. In Section 5, we briefly review the basic notions of energy loss and jet quenching that are used in our study. In Section 6, we describe how we study the medium modification of jet fragmentation at RHIC and LHC. Finally, we discuss in Section 7 our results and what we plan to study in the future using the recombination model developed in the present study.

2. HADRONIZATION

2.1 Fragmentation of Jets into Hadrons

Partons such as quarks and gluons produced in nuclear collisions cannot exist alone due to color confinement. They soon form hadrons that are measured in detectors. Because of its non-perturbative nature, the hadronization process is usually described by phenomenological fragmentation functions $D_i^h(z_i, Q^2_{\rm hard})$ defined as the differential probability for a parton i (quark or gluon) to fragment into a hadron h carrying a fraction z of its momentum. Although the perturbative QCD can be used to treat the hard process for initial jet production due to its large energy scale, it is not applicable for describing hadron production. However, the factorization theorem allows us to separate the cross section for the hard process and the fragmentation function, which can be parameterized from experimental measurements and is universal for the process [12]. Hence, the differential cross section for the production of h carrying energy E_h in a process $a + b \to h + X$ can be written as

$$\frac{d\sigma}{dE_h}(ab \to hX) = \sum_i \int \frac{d\sigma}{dE_i}(ab \to iX) D_i^h(z_i, Q^2_{\rm hard}) \frac{dE_i}{E_i}, \tag{2.1}$$

where $d\sigma/dE_i$ is the differential cross section for the production of a parton i with energy E_i, $Q^2_{\rm hard}$ is the scale of the hard process, and $z_i = E_h/E_i$ $(0 \le z_i \le 1)$. In order to obtain hadron distributions from those of partons, each parton is assumed to fragment into hadrons independently with the color structure ignored. Such an independent fragmentation model was pioneered by Field and Feynman [13].

In the PYTHIA, which is a Monte Carlo event generator, the string fragmentation shown in Fig. 2.1 is the main tool used for the hadronization of parton showers [22].

Unlike an electric field, a color field caused by a $q\bar{q}$ pair is restricted in a narrow space due to the gluon self-interaction, forming thus a string-like object. The string has

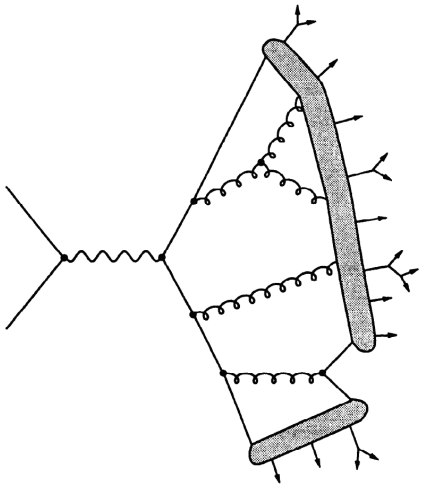

Figure 2.1: Hadronization of parton shower by string fragmentation. Figure adapted from Ref. [1]

a uniform energy per unit length. It leads to the linear color confining potential, i.e. $V \sim \kappa r$, where the string tension κ is approximately 1 GeV/fm [23, 24, 25, 26, 27]. As the separation of the $q\bar{q}$ pair increases, the string breaks into hadron-sized pieces through spontaneous $q\bar{q}$ pair production in its color field, and the original pair is divided into two color neutral systems. The colorless systems can form mesons if their invariant masses are small, otherwise they produce additional $q\bar{q}$ pairs through string breaking. Quantum mechanically, the quark and antiquark are created at the same point and then tunnel out to the classically allowed region according to the Schwinger mechanism [28]. The tunneling probability is given by

$$\mathcal{P} = \exp\Big(-\frac{\pi m_\perp^2}{\kappa}\Big) = \exp\Big(-\frac{\pi m^2}{\kappa}\Big)\exp\Big(-\frac{\pi p_\perp^2}{\kappa}\Big), \tag{2.2}$$

where $m_\perp = \sqrt{m^2 + p_\perp^2}$ is the transverse mass of the quark and antiquark. It gives a Gaussian distribution for the transverse momentum. The total $p_\perp$ of the $q\bar{q}$ pair should vanish due to momentum conservation.

The string fragmentation is very similar to the independent fragmentation for a simple quark-antiquark system. However, two models differ significantly when gluons are present [27]. In string fragmentation, the gluon is considered as a kink in the string with the quark and antiquark forming the kink carrying a localized energy and momentum equal to that of the gluon. The fragmentation of the system then behaves in the same way as in the case of the quark-antiquark string.

There is another well-known fragmentation model called the cluster fragmentation that is used in the Monte Carlo event generator HERWIG [2]. As shown in the

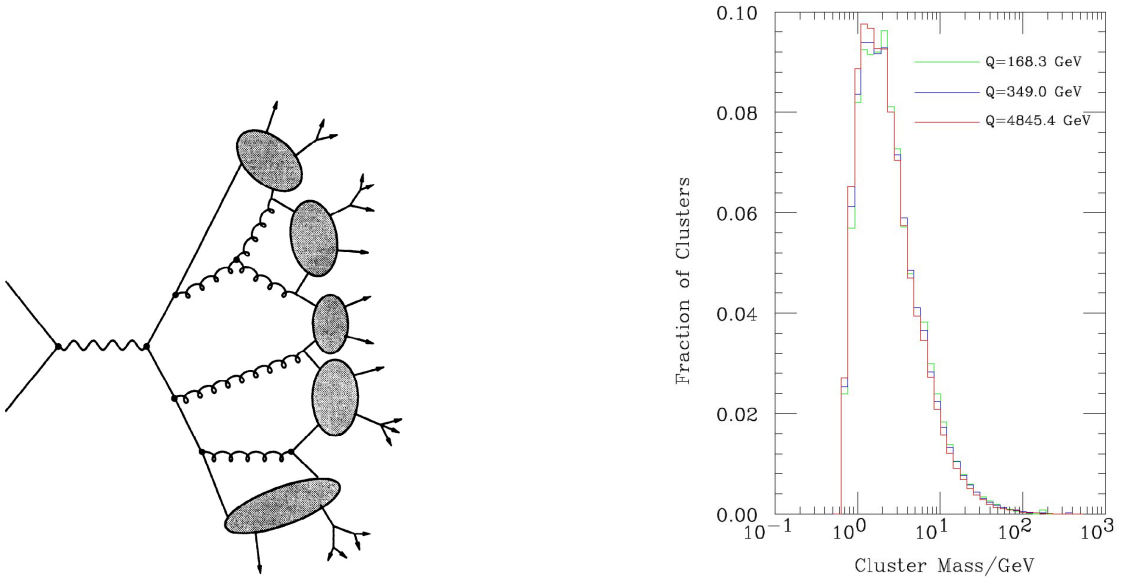

Figure 2.2: (Left) Hadronization of parton shower by cluster fragmentation. Figure adapted from Ref. [1]. (Right) Universal cluster mass spectrum. Figure adapted from Ref. [2].

left figure of Fig. 2.2, jets produced from the hard scattering are perturbatively branched into shower partons, and all outgoing gluons are forced to nonperturbatively decay into quark-antiquark or diquark-antidiquark pairs. Neighboring quarks and antiquarks not from the same decayed gluons then combine into color-singlet *clusters*. Due to color *preconfinement* [29], these clusters have a distribution of masses and spatial sizes that peaks at low values, drops rapidly with the cluster mass and size, and is asymptotically independent of the hard subprocess type and scale (see the right figure of Fig. 2.2). Since each cluster has to decay into a pair of hadrons, masses of clusters must be sufficiently large.

2.2 Recombination of Jet Shower Partons into Hadrons

The recombination model was introduced to explain unexpected observations such as the baryon puzzle in relativistic heavy ion collisions [30, 31], which is related to the enhanced baryon production in the intermediate momentum region. The coalescence model gives a good explanation for the baryon anomaly at RHIC [14, 32, 33, 34, 35]. The basic idea in the recombination model is to calculate the instantaneous projection of parton states onto hadron states [36]. The importance of the quark recombination model was demonstrated in the works by three theoretical collaborations; Fries, Müller, Nonaka, and Bass (FMNB) [15, 35], Greco, Ko, and Lévai (GKL) [11, 14], and Hwa and Yang (HY) [16, 37].

Here, we briefly review the HY approach because unlike other approaches, it uses shower partons for the recombination. In this approach, the shower parton distribution (SPD) is, however, extracted from fitting the measured hadron spectra [16]. Also, instead of carrying out the recombination calculation in three-dimensional (3D) space and time as well as in three-dimensional momentum, Hwa and Yang only considered the momentum in one-dimension (1D) by allowing collinearly moving

partons to recombine. The invariant inclusive spectra for produced mesons and baryons [16] are then given by

$$p\frac{dN_M}{dp} = \int \frac{dp_1}{p_1}\frac{dp_2}{p_2} F_{q\bar{q}'}(p_1, p_2) R_M(p_1, p_2, p), \tag{2.3}$$

$$p\frac{dN_B}{dp} = \int \frac{dp_1}{p_1}\frac{dp_2}{p_2}\frac{dp_3}{p_3} F_{q_1 q_2 q_3}(p_1, p_2, p_3) R_B(p_1, p_2, p_3, p), \tag{2.4}$$

where $F_{q\bar{q}}(p_1, p_2)$ is the joint distribution for a quark of momentum p_1 and an antiquark of momentum p_2, $F_{q_1 q_2 q_3}(p_1, p_2, p_3)$ is that for three quarks of momenta p_1, p_2, and p_3, and R_M and R_B are the recombination functions (RF) for the processes $q\bar{q} \to M$ and $q_1 q_2 q_3 \to B$, respectively. For the thermal parton distribution, they used the fact that observed meson distribution $dN_M/(pdp)$ at low p follows an exponential law. Employing this approach, they have shown that the recombination of shower partons with thermal partons dominates in the momentum range $3 < p_T < 8$ GeV. However, as we mentioned above, their shower partons are not obtained from a real Monte Carlo event generator but are extracted from fitting the experimental data.

3. JETS AND PARTON SHOWER EVOLUTION

Highly collimated sprays of particles produced in the hard scattering of a high energy collision are called *jets*. Jets are the signature of hard scattering processes. Since jets of energetic partons contain a large scale, their behaviors in vacuum can be described by the perturbative QCD, which makes them good probes to study the medium produced in ultra-relativistic heavy ion collisions. While evolving in vacuum and/or medium, the energetic jets can radiate. There are two traditional approaches to the modeling of perturbative processes.

One is the matrix-element method [22], in which Feynman diagrams are calculated order by order. In principle, this method is the correct approach because exact kinematics, full interference, and the helicity structure can be taken into account. However, the calculation of Feynman diagrams becomes extremely complicated when going to high orders. Therefore, the second approach, called the parton-shower approach, has been suggested. In the parton-shower approach, several splittings or branchings of one parton into two are combined to produce a shower of partons. The shower-parton approach gives a good description of the evolution of a jet because the resulting parton showers are confined in a narrow angle around the leading jet as observed in experiments. A moving parton from the hard scattering thus reduces its virtualities by radiating shower partons. In the shower parton formulation, the kinematics of each branching is determined by two variables, the virtuality Q^2 of the branching parton and the momentum fraction z carried by the daughter parton. This can have different interpretations in different shower algorithms. In our study, we use PYTHIA 6.4 [22], which is a Monte Carlo event generator, to generate shower partons from jets in vacuum. The probability for a parton to branch into two partons

is given by the evolution equations called the DGLAP (Dokshitzer-Gribov-Lipatov-Altarelli-Parisi) [38, 39, 40] equation given by

$$d\mathcal{P}_{a\to bc} = \frac{\alpha_s}{2\pi}\frac{dQ^2}{Q^2}P_{a\to bc}(z)dz, \tag{3.1}$$

where a, b, and c denote the mother and daughter particles, respectively, and z gives the fraction of momentum carried by daughter b with respect to the momentum of mother a. There are three possible splitting kernels $q \to qg$, $g \to q\bar{q}$, and $g \to gg$ whose probabilities are:

$$P_{q\to qg}(z) = \frac{4}{3}\frac{1+z^2}{1-z}, \tag{3.2}$$

$$P_{g\to gg}(z) = 3\frac{(1-z(1-z))^2}{z(1-z)}, \tag{3.3}$$

$$P_{g\to q\bar{q}}(z) = \frac{N_f}{2}(z^2+(1-z)^2). \tag{3.4}$$

Introducing the variable t,

$$t = \ln(Q^2/\Lambda^2), \quad \mathrm{d}t = \mathrm{d}\ln(Q^2) = \mathrm{d}Q^2/Q^2, \tag{3.5}$$

in terms of the QCD scale Λ, which gradually decreases during the evolution of partons in the final-state showers, we can define the Sudakov form factor [41]

$$S_a(T) \equiv \mathcal{P}_{\text{nothing}}(0,T) = \exp\Big(-\int_0^T dt\frac{d\mathcal{P}_{\text{something}}(t)}{dt}\Big), \tag{3.6}$$

which gives the probability that a parton will not branch during the evolution from

0 to T. The DGLAP equations can then be rewritten as

$$d\mathcal{P}_{a\to bc} = \frac{\alpha_s}{2\pi}\frac{dQ^2}{Q^2}P_{a\to bc}(z)dz\exp\Big(-\sum_{b,c}\int_{Q^2}^{Q^2_{\max}}\frac{dQ'^2}{Q'^2}\int_{z_-(Q'^2)}^{z_+(Q'^2)}\frac{\alpha_s}{2\pi}P_{a\to bc}(z')dz'\Big), \quad (3.7)$$

where $Q_{\max}$ is the initial maximum virtuality of the jet parton. We note that $d\mathcal{P}_{a\to bc}$ is normalized according to $\sum_{b,c}\int dQ^2\int dz d\mathcal{P}_{a\to bc} \equiv 1$. In general, the initial virtuality Q_i for generating the final-state parton showers are determined by the hard scattering. The momentum fraction carried by the daughter parton is restricted to

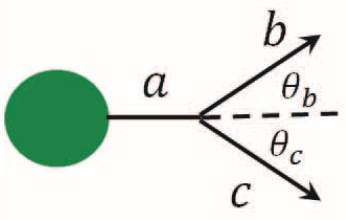

Figure 3.1: Splitting of a shower parton.

a certain region. For example, for a parton of virtuality $Q^2 = p^2 = E^2 - \mathbf{p}^2$ branching into two partons b and c as shown in Fig. 3.1, the kinematics of this process $a \to b+c$ gives the following relations for the four-momenta of the partons [42]:

$$p_{a\mu} = (E_a, \mathbf{0}, p_a), \quad p_a^2 = E_a^2 - Q_a^2 \quad (3.8)$$

$$p_{b\mu} = (zE_z, \mathbf{k}_\perp, p_a), \quad p_{b\mu}p_b^\mu = z^2E_a^2 - k_\perp^2 - p_b^2 = Q_b^2 \quad (3.9)$$

$$p_{c\mu} = ((1-z)E_a, -\mathbf{k}_\perp, p_a - p_b)$$

$$p_{c\mu}p_c^\mu = (1-z)^2E_a^2 - k_\perp^2 - (p_a - p_b)^2 = Q_c^2. \quad (3.10)$$

These relations yield

$$p_b = \frac{2zE_a^2 - Q_a^2 - Q_b^2 + Q_c^2}{2p_a} \tag{3.11}$$

$$k_\perp^2 = -z^2\frac{Q_a^2E_a^2}{p_a^2} - z\frac{E_a^2}{p_a^2}(Q_c^2 - Q_a^2 - Q_b^2) - \frac{(Q_c^2 - Q_a^2 - Q_b^2)^2}{4p_a^2} - Q_b^2. \tag{3.12}$$

If one assumes that the momenta of partons are much larger than their virtualities, the transverse momentum can be rewritten as

$$k_\perp^2 \approx z(1-z)Q_a^2 - (1-z)Q_b^2 - zQ_c^2 \approx z(1-z)Q_a^2. \tag{3.13}$$

The opening angle $\theta_a = \theta_b + \theta_c$ in Fig. 3.1 is approximately given by

$$\theta_a \approx \frac{k_\perp}{p_b} + \frac{k_\perp}{p_c} \approx \frac{\sqrt{z(1-z)}Q_a}{zE_a} + \frac{\sqrt{z(1-z)}Q_a}{(1-z)E_a} = \frac{Q_a}{\sqrt{z(1-z)}E_a}. \tag{3.14}$$

Eq. (3.13) is employed in the subroutine PYSHOW of PYTHIA 6.4 for generating parton showers based on the mass-ordering ($Q_a^2 >> Q_b^2, Q_c^2$). Solving the kinematic equations, we have

$$z_\pm = \frac{1}{2}\left\{1 + \frac{Q_b^2 - Q_c^2}{Q_a^2} \pm \frac{|\mathbf{p}_a|}{E_a}\frac{\sqrt{(Q_a^2 - Q_b^2 - Q_c^2)^2 - 4Q_b^2Q_c^2}}{Q_a^2}\right\}, \tag{3.15}$$

which gives the allowed range of z.

In the following, we describe how to build a parton shower generator by using the Monte Carlo method and the Sudakov form factor. Given the virtuality scale ($t = \ln(Q^2/\Lambda^2)$) and momentum fraction (t_1, x_1) after several steps in the evolution, or as initial conditions, one can generate the values of (t_2, x_2) in the next step as shown in Fig. 3.2. The probability of evolving from t_1 to t_2 without branching is

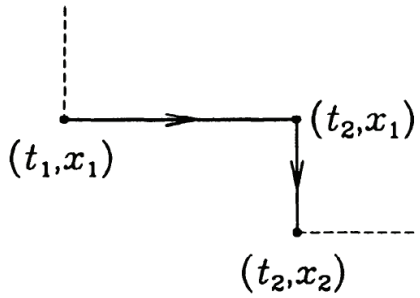

Figure 3.2: Fundamental step in (t, x)-space. Figure adapted from Ref. [1].

$\Delta(t_2)/\Delta(t_1)$, where $\Delta(t)$ is the Sudakov form factor for the process $i \to j$ written as

$$\Delta_i(t) \equiv \exp\left[-\sum_j \int_{t_0}^{t} \frac{dt'}{t'} \int dz \frac{\alpha_s}{2\pi} \hat{P}_{ji}(z)\right]. \tag{3.16}$$

Hence, t_2 is generated with a probability distribution obtained from solving the equation $\Delta(t_1)/\Delta(t_2) = \mathcal{R}$, where $\mathcal{R}$ is a random number generated uniformly in the interval $[0, 1]$. If t_2 is smaller than the minimum cutoff value for the mass scale t_0, no further branching occurs. Otherwise, we obtain the momentum fraction $z = x_1/x_2$ for the next branching with a probability distribution proportional to $(\alpha_s/2\pi)P(z)$, where $P(z)$ is the appropriate splitting function for the process. This can be obtained from the solution of the equation

$$\int_{\epsilon}^{x_1/x_2} \mathrm{d}z \frac{\alpha_s}{2\pi} P(z) = \mathcal{R}' \int_{\epsilon}^{1-\epsilon} \mathrm{d}z \frac{\alpha_s}{2\pi} P(z), \tag{3.17}$$

where $\mathcal{R}'$ represents another random number in the interval $[0, 1]$, and ϵ is the infrared cut-off for resolvable branching. As a consequence of successive branching, a parton evolves. Each outgoing branched parton becomes the source of a new branching until the Monte Carlo algorithm generates a 'non-branching' step in the evolution

of its virtual mass. Finally, all outgoing partons cease to evolve when their virtualities reach the cutoff scale t_0. At this stage, they will be converted to hadrons.

4. JET FRAGMENTATION VIA SHOWER PARTON RECOMBINATION*

*As described in Section 2, hadron production from energetic jets in high-energy nuclear collisions is usually parameterized through the fragmentation functions due to the universality of the process as given by QCD factorization theorems [12]. On a more microscopic level, we can achieve a good description of jet hadronization through a perturbative evolution of the parton showers inside the jet using DGLAP splitting kernels from the largest momentum scale to some lower cutoff Q_0, followed by a non-perturbative hadronization model like the Lund string model applied to the parton shower. The Monte Carlo based event generators like PYTHIA [22] and HERWIG [43] have successfully implemented such strategies to describe high momentum hadron production in $e^+ + e^-$, $p + p$, and other processes.

In collisions of heavy nuclei at high energy, QCD factorization in jet hadronization breaks down at significantly higher hadron momentum, approximately 6-8 GeV/c at typical collider energies, compared to the situation in elementary $e^+ + e^-$ and $p + p$ collisions. The baryon enhancement observed in nuclear collisions both in Au+Au collisions at RHIC [44] and in Pb+Pb collisions at LHC [5] is an evidence for this effect. It has been suggested that hadron production at intermediate momentum, i.e. 2-8 GeV/c, can be described through the process of quark recombination or coalescence [11, 14, 15, 35, 45]. It is an intriguing idea to combine the concepts of quark recombination and parton showers since it would easily generalize to the hadronization of jets in dense environments as in relativistic heavy ion collisions. Hwa and Yang have pioneered the application of quark recombination to jet showers

*The major part of this section is reprinted with permission from "Jet fragmentation via recombination of Parton Showers" by K. C. Han, R. J. Fries, and C.-M. Ko, 2016. Physical Review C93 (2016) no.4, 045207 by Physical Review C. Available at http://journals.aps.org/prc/abstract/10.1103/PhysRevC.93.045207.

in Ref. [16]. However, the parton showers in their work were not obtained from first principles but fitted to measured hadron spectra. They also ignored the smallness of the number of partons in each jet by applying recombination to averaged spectra instead of event-by-event showers.

Here we show that essential aspects of hadron production from parton showers in jet can be reproduced if we substitute an improved recombination model for the Lund string fragmentation in PYTHIA. For this work, we obtain quarks and gluons generated at the end of their DGLAP based perturbative shower evolution in PYTHIA and let gluons decay into quark-antiquark pairs. We evaluate the quark recombination probabilities based on the hadron Wigner functions by Monte Carlo sampling and finally reapply Lund string fragmentation to those quarks that cannot find their partner for the recombination. We then compare our results with those from the full PYTHIA in which the entire parton showers are converted to hadrons by string fragmentation.

4.1 Parton Showers from Electron-Positron Annihilation in PYTHIA

First of all, we use PYTHIA 6.3 [22] to generate an ensemble of parton showers by selecting 2-jet events in $e^+ + e^-$ collisions at different center-of-mass energies $\sqrt{s} = 2E_{\rm jet}$. By setting the cutoff for the perturbative evolution of the jet to $Q_0 = 1$ GeV, we extract the final parton configuration before string breaking in PYTHIA. The upper panels of Fig. 4.1 show the light quark $(u, d, \bar{u}, \bar{d})$, strange quark $(s, \bar{s})$ and gluon (g) spectra of $E_{\rm jet} = 100$ GeV jets as functions of their longitudinal momentum fraction z and transverse momentum $\mathbf{p}_T$ with respect to the jet axis,

$$z = \frac{\mathbf{p} \cdot \mathbf{P}_{\rm jet}}{|\mathbf{P}_{\rm jet}|^2}, \quad |\mathbf{p}_T| = \frac{\sqrt{p^2 P_{\rm jet}^2 - (\mathbf{p} \cdot \mathbf{P}_{\rm jet})^2}}{P_{\rm jet}} \tag{4.1}$$

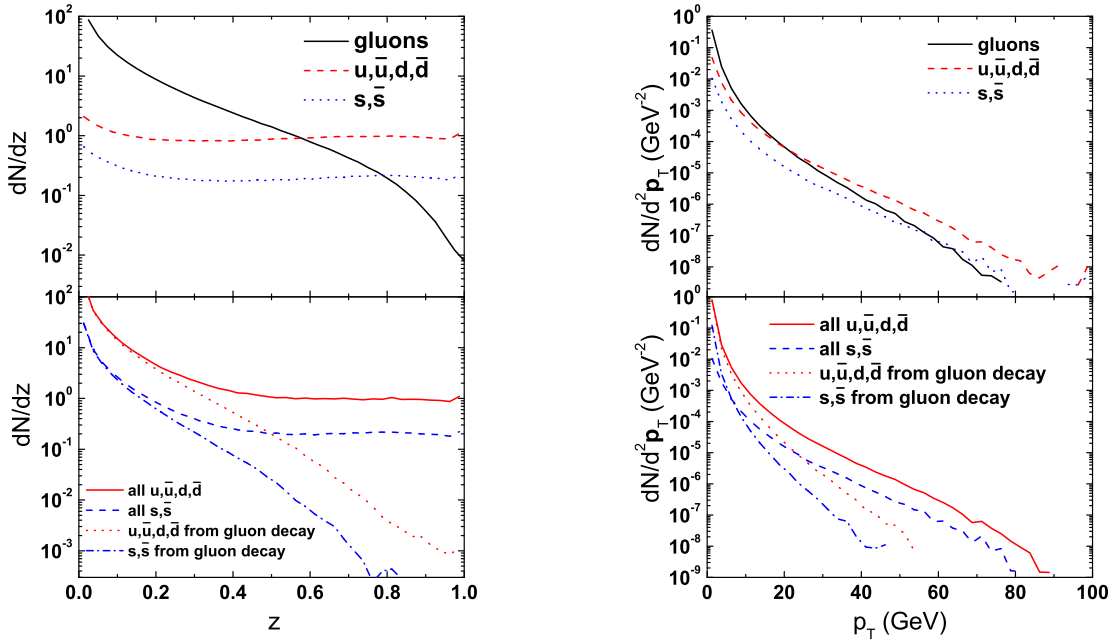

Figure 4.1: Upper panels: Distribution of shower partons in terms of the momentum fraction z (left) and the transverse momentum p_T (right) of the initial jet momentum at the end of the perturbative shower evolution for a sample of 10^6 jets of 100 GeV each. Lower panels: The same after forcing gluon decays into quark-antiquark pairs as described in the text. Figures adapted from Ref. [3].

where $\mathbf{p}$ is the parton 3-momentum vector and $\mathbf{P}_{\rm jet}$ is the 3-momentum of the original parton creating the jet. The spectrum dN/dz and $dN/d^2\mathbf{p}_T$ here is normalized to one jet, and all jets shown in the sample have $P_{\rm jet} = 100$ GeV.

Let us emphasize that perturbative parton shower spectra here are simply an input in our hadronization model, not part of it. We will use the same parton shower sample as input to Lund string fragmentation, and the relevant observables will be the difference between both hadronization modes.

Recombination models are usually built on the premise of dominance of the lowest Fock states in hadron wave functions, similar to hadronization in exclusive processes, and thus only quarks and antiquarks are considered (see Ref. [46] for a study on

higher Fock states). Successful recombination models therefore postulate a (non-perturbative) splitting of gluons into quark-antiquark pairs. We use constituent quarks with masses $m_{u,d} = 0.33$ GeV for light quarks and $m_s = 0.5$ GeV for strange quarks, consistent with PYTHIA.

Gluons at the end of their perturbative evolution are allowed to have virtualities between $2m_{u,d}$ and $m_{\max}$, where $m_{\max} > 2m_s$ should not be much larger than the scale Q_0, and its value will mostly influence the ratio of strange to non-strange hadrons. We will set this parameter to 1.25 GeV throughout this work. Gluons are then forced to decay isotropically into a $q\bar{q}$ pair in the gluon rest frame. The decay chemistry gives equal weight to $u\bar{u}$ and $d\bar{d}$ pairs for gluon virtualities between $2m_{u,d}$ and $2m_s$ while above the strangeness threshold the ratio of light to strange quarks is simply given by phase space and the vector nature of the decay as

$$\frac{\Gamma(g^* \to u\bar{u}, d\bar{d})}{\Gamma(g^* \to s\bar{s})} = 2\frac{m^2 + 2m_{u,d}^2}{m^2 + 2m_s^2}\sqrt{\frac{m^2 - 4m_{u,d}^2}{m^2 - 4m_s^2}}\,. \tag{4.2}$$

The derivation of the above ratio is given in APPENDIX A. We do not consider heavy quarks in this study.

PYTHIA forces the final virtuality of shower gluons to zero when the value becomes smaller than Q_0. While one could in principle undo this step, it turns out to be absolutely sufficient to reintroduce the non-perturbative gluon virtuality manually without rebalancing momenta in the last splitting. We find the typical error in total energy of the shower introduced this way is less than 1% for 100 GeV jets. The lower panel of Fig. 4.1 shows the spectra of light and strange quarks from gluon decays for the same sample of 100 GeV jets, together with the total light and strange quark spectra.

In principle, quark recombination could be formulated completely in momentum

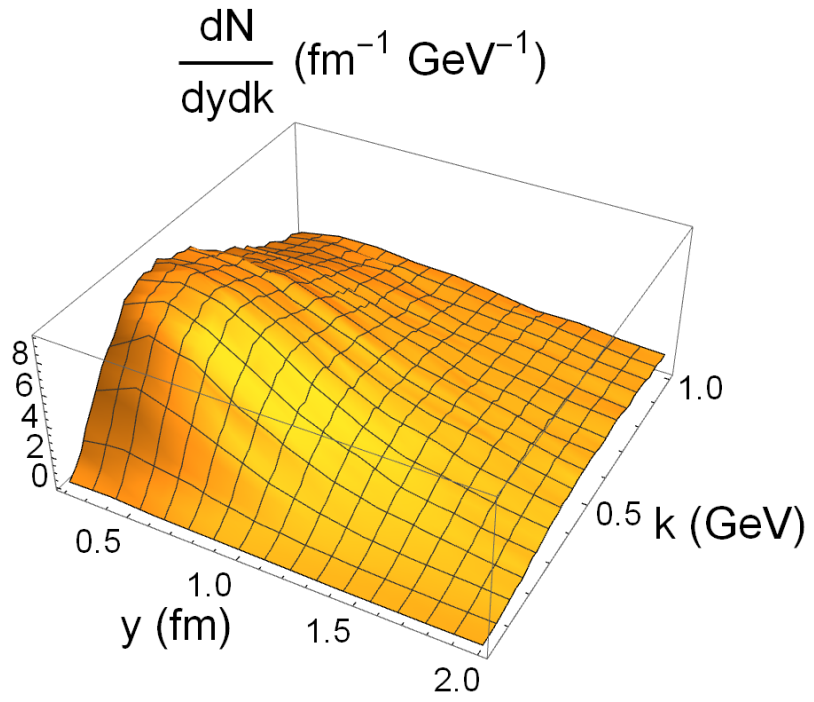

Figure 4.2: Relative spatial and momentum distributions of all quark-antiquark pairs at their center-of-mass frame. Figure adapted from Ref. [3].

space (see Ref. [47]) for applications to jet showers. However, for future applications in heavy ion collisions, the available distribution of thermal partons will be a function of space-time coordinates and hence we espouse a formulation of quark recombination employing Wigner functions with both momentum and space-time information. We are therefore led to introduce a space-time structure of showers. We do this based on two simple premises: (i) Virtual partons with virtuality Q have an average lifetime $1/Q$ in their rest frame before splitting. This time is then properly boosted into the lab frame. (ii) The centers of wave packets representing partons move on free classical trajectories given by the velocity $\mathbf{p}/E$ of the parton in the lab frame, where E is the parton energy.

In the jet rest frame the spatial density of its shower partons depends on the time

they are produced. However their density in momentum space is about $0.025/\mathrm{GeV}^3$ and significantly smaller than the corresponding value of about $2.5/\mathrm{GeV}^3$ for partons in a quark-gluon plasma at its phase transition temperature. One can analyze this parton initial state for hadronization more quantitatively. As we will discuss in detail in the next section, the relevant physical quantities for recombination between a quark and antiquark pair are their relative separation y and relative momentum k at a common time in their rest frame. In Fig. 4.2 we show the statistical distribution of all quark-antiquark pairs we find in 100 GeV jet parton showers (normalized to one jet) as a function of their distances y and k in their common rest frame at the time when the latter parton of a pair is created. We find that this distribution peaks at $y \sim 0.5$ fm and $k \sim 0.3$ GeV, although large tails exist. This points to the existence of a "bulk" of partons in a jet shower which are quite close in phase space and amenable to recombination, while another, non-negligible fraction of partons will be far removed from other partons in phase space.

4.2 Quark Recombination

In the recombination model, the probabilities of partons to recombine into hadrons are determined by the overlap between the phase spaces of a quark-antiquark (or three quark) state and a meson (or a baryon) based on the sudden approximation. Now, we calculate the overlap between a quark-antiquark state and a meson. We suppose that the wave functions of quark and antiquark and meson in a volume V are given, respectively, by

$$\langle \mathbf{r}_1, \mathbf{r}_2 | i \rangle = \phi_q(\mathbf{r}_1)\phi_{\bar{q}}(\mathbf{r}_2) \tag{4.3}$$

$$\langle \mathbf{r}_1, \mathbf{r}_2 | f \rangle = \frac{1}{\sqrt{V}} e^{i\mathbf{K}_M \cdot (\mathbf{r}_1 + \mathbf{r}_2)/2} \Phi_M(\mathbf{r}_1 - \mathbf{r}_2), \tag{4.4}$$

where $\mathbf{r}_1$ and $\mathbf{r}_2$ are the coordinates of the quark and antiquark, $\Phi_M(\mathbf{r}_1, \mathbf{r}_2)$ gives the internal wave function of the meson, and $\mathbf{K}_M$ is its momentum. The probability for the recombination of quark and antiquark into the meson is calculated by the squared overlap amplitude

$$\begin{aligned}
\mathcal{P} &= \sum_{\mathbf{K}_M} |\langle f|i\rangle|^2 = \sum_{\mathbf{K}_M} \int d^3\mathbf{r}_1 d^3\mathbf{r}_2 d^3\mathbf{r}'_1 d^3\mathbf{r}'_2 \langle f|\mathbf{r}_1, \mathbf{r}_2\rangle\langle \mathbf{r}_1, \mathbf{r}_2|i\rangle\langle i|\mathbf{r}'_1, \mathbf{r}'_2\rangle\langle \mathbf{r}'_1, \mathbf{r}'_2|f\rangle \\
&= V \int \frac{d^3\mathbf{K}_M}{(2\pi)^3} d^3\mathbf{r}_1 d^3\mathbf{r}_2 d^3\mathbf{r}'_1 d^3\mathbf{r}'_2 \frac{1}{V} e^{-i\mathbf{K}_M\cdot(\mathbf{r}_1+\mathbf{r}_2)/2} \Phi^*_M(\mathbf{r}_1 - \mathbf{r}_2)\phi_q(\mathbf{r}_1)\phi_{\bar{q}}(\mathbf{r}_2) \\
&\times \phi^*_q(\mathbf{r}'_1)\phi^*_{\bar{q}}(\mathbf{r}'_2) e^{i\mathbf{K}_M\cdot(\mathbf{r}'_1+\mathbf{r}'_2)/2} \Phi_M(\mathbf{r}'_1 - \mathbf{r}'_2). \qquad (4.5)
\end{aligned}$$

where $\sum_{\mathbf{K}_M} = V \int \frac{d^3\mathbf{K}_M}{(2\pi)^3}$ has been used. Defining the new coordinates

$$\begin{aligned}
\mathbf{x}_1 = \frac{\mathbf{r}_1 + \mathbf{r}'_1}{2}; \quad \mathbf{x}_2 = \frac{\mathbf{r}_2 + \mathbf{r}'_2}{2} \\
\mathbf{y}_1 = \mathbf{r}_1 - \mathbf{r}'_1; \quad \mathbf{y}_2 = \mathbf{r}_2 - \mathbf{r}'_2, \qquad (4.6)
\end{aligned}$$

we can write

$$\begin{aligned}
\mathcal{P} &= \int \frac{d^3\mathbf{K}_M}{(2\pi)^3} d^3\mathbf{x}_1 d^3\mathbf{x}_2 d^3\mathbf{y}_1 d^3\mathbf{y}_2 e^{-i\mathbf{K}_M\cdot(\mathbf{y}_1+\mathbf{y}_2)/2} \Phi^*_M \left(\mathbf{x}_1 + \frac{\mathbf{y}_1}{2} - \mathbf{x}_2 - \frac{\mathbf{y}_2}{2}\right) \\
&\times \phi_q\left(\mathbf{x}_1 + \frac{\mathbf{y}_1}{2}\right) \phi_{\bar{q}}\left(\mathbf{x}_2 + \frac{\mathbf{y}_2}{2}\right) \phi^*_q\left(\mathbf{x}_1 - \frac{\mathbf{y}_1}{2}\right) \phi^*_{\bar{q}}\left(\mathbf{x}_2 - \frac{\mathbf{y}_2}{2}\right) \\
&\times \Phi_M\left(\mathbf{x}_1 - \frac{\mathbf{y}_1}{2} - \mathbf{x}_2 + \frac{\mathbf{y}_2}{2}\right). \qquad (4.7)
\end{aligned}$$

In terms of the Wigner functions of quark and antiquark [48]

$$W_{q,\bar{q}}(\mathbf{x}_i, \mathbf{k}_i) = \int d^3\mathbf{y}_i \phi^*_{q,\bar{q}}\left(\mathbf{x}_i - \frac{\mathbf{y}_i}{2}\right) \phi_{q,\bar{q}}\left(\mathbf{x}_i + \frac{\mathbf{y}_i}{2}\right) e^{-i\mathbf{k}_i\cdot\mathbf{y}_i}, \qquad (4.8)$$

with $i = 1$ for the quark and $i = 2$ for the antiquark, we have

$$\phi^*_{q,\bar{q}}\left(\mathbf{x}_i - \frac{\mathbf{y}_i}{2}\right)\phi_{q,\bar{q}}\left(\mathbf{x}_i + \frac{\mathbf{y}_i}{2}\right) = \int \frac{d^3\mathbf{k}_i}{(2\pi)^3} W_{q,\bar{q}}(\mathbf{x}_i, \mathbf{k}_i) e^{i\mathbf{k}_i\cdot\mathbf{y}_i}. \tag{4.9}$$

Similarly, for the meson wave function, we can write

$$\begin{aligned}\Phi^*_M\left((\mathbf{x}_1 - \mathbf{x}_2) + \frac{\mathbf{y}_1 - \mathbf{y}_2}{2}\right)\Phi_M\left((\mathbf{x}_1 - \mathbf{x}_2) - \frac{\mathbf{y}_1 - \mathbf{y}_2}{2}\right)\\ = \int \frac{d^3\mathbf{k}}{(2\pi)^3} W_M(\mathbf{x}_1 - \mathbf{x}_2, \mathbf{k}) e^{-i\mathbf{k}\cdot(\mathbf{y}_1 - \mathbf{y}_2)},\end{aligned} \tag{4.10}$$

where $W_M(\mathbf{x}_1 - \mathbf{x}_2, \mathbf{k})$ is the Wigner function of the meson. We note that both the quark and the meson Wigner functions are normalized as $(2\pi)^{-3}\int d^3\mathbf{x}d^3\mathbf{k}W(\mathbf{x},\mathbf{k}) = 1$.

Inserting Eqs. (4.9) and (4.10) into Eq. (4.7), we can write the probability as

$$\begin{aligned}\mathcal{P} &= \int \frac{d^3\mathbf{K}_M}{(2\pi)^3} d^3\mathbf{x}_1 d^3\mathbf{x}_2 d^3\mathbf{y}_1 d^3\mathbf{y}_2 \frac{d^3\mathbf{k}_1}{(2\pi)^3}\frac{d^3\mathbf{k}_2}{(2\pi)^3}\frac{d^3\mathbf{k}}{(2\pi)^3} e^{-i\mathbf{K}_M\cdot\frac{\mathbf{y}_1+\mathbf{y}_2}{2}}\\
&\times W_q(\mathbf{x}_1, \mathbf{k}_1) e^{i\mathbf{k}_1\cdot\mathbf{y}_1} W_{\bar{q}}(\mathbf{x}_2, \mathbf{k}_2) e^{i\mathbf{k}_2\cdot\mathbf{y}_2} W_M(\mathbf{x}_1 - \mathbf{x}_2, \mathbf{k}) e^{-i\mathbf{k}\cdot(\mathbf{y}_1 - \mathbf{y}_2)}\\
&= \int \frac{d^3\mathbf{K}_M}{(2\pi)^3} d^3\mathbf{x}_1 d^3\mathbf{x}_2 \frac{d^3\mathbf{k}_1 d^3\mathbf{k}_2 d^3\mathbf{k}}{(2\pi)^3}\delta^3\left(-\frac{\mathbf{K}_M}{2} + \mathbf{k}_1 - \mathbf{k}\right)\delta^3\left(-\frac{\mathbf{K}_M}{2} + \mathbf{k}_2 + \mathbf{k}\right)\\
&\times W_q(\mathbf{x}_1, \mathbf{k}_1) W_{\bar{q}}(\mathbf{x}_2, \mathbf{k}_2) W_M(\mathbf{x}_1 - \mathbf{x}_2, \mathbf{k})\\
&= \int \frac{d^3\mathbf{K}_M}{(2\pi)^3} d^3\mathbf{x}_1 d^3\mathbf{x}_2 \frac{d^3\mathbf{k}_1 d^3\mathbf{k}_2}{(2\pi)^3} W_q(\mathbf{x}_1, \mathbf{k}_1) W_{\bar{q}}(\mathbf{x}_2, \mathbf{k}_2)\\
&\times W_M\left(\mathbf{x}_1 - \mathbf{x}_2, \frac{\mathbf{k}_1 - \mathbf{k}_2}{2}\right)\delta^3(\mathbf{k}_1 + \mathbf{k}_2 - \mathbf{K}_M).\end{aligned} \tag{4.11}$$

Changing Eq. (4.11) into a differential form, we have

$$\frac{d\mathcal{P}}{d^3\mathbf{K}_M} = \int \frac{d^3\mathbf{x}_1 d^3\mathbf{k}_1}{(2\pi)^3}\frac{d^3\mathbf{x}_2 d^3\mathbf{k}_2}{(2\pi)^3} W_q(\mathbf{x}_1, \mathbf{k}_1) W_{\bar{q}}(\mathbf{x}_2, \mathbf{k}_2) W_M(\mathbf{y}, \mathbf{k})\, \delta^3(\mathbf{K}_M - \mathbf{k}_1 - \mathbf{k}_2), \tag{4.12}$$

where we have defined $\mathbf{y} = \mathbf{x}_1 - \mathbf{x}_2$ and $\mathbf{k} = \frac{\mathbf{k}_1 - \mathbf{k}_2}{2}$. Eq. (4.12) gives the probability of a quark and antiquark pair to recombine into a meson of momentum $\mathbf{K}_M$.

For a system of quarks and antiquarks of phase-space distributions $f_q(\mathrm{x}, \mathrm{k})$ and $f_{\bar{q}}(\mathrm{x}, \mathrm{k})$, respectively, with normalizations $\int d^3\mathbf{x} d^3\mathbf{k} f_{q,\bar{q}}(\mathbf{x}, \mathbf{k}) = N_{q,\bar{q}}$, the momentum spectrum of mesons formed from the recombination of these quarks and antiquarks is then given by

$$\frac{dN_M}{d^3\mathbf{K}_M} = g_M \int d^3\mathbf{x}_1 d^3\mathbf{k}_1 d^3\mathbf{x}_2 d^3\mathbf{k}_2 f_q(\mathbf{x}_1, \mathbf{k}_1) f_{\bar{q}}(\mathbf{x}_2, \mathbf{k}_2) \overline{W}_M(\mathbf{y}, \mathbf{k}) \delta^{(3)}(\mathbf{K}_M - \mathbf{k}_1 - \mathbf{k}_2). \tag{4.13}$$

In the above, $\overline{W}_M(\mathbf{y}, \mathbf{k})$ is the overlap integral of quark and meson Wigner functions,

$$\overline{W}_M(\mathbf{y}, \mathbf{k}) = \int \frac{d^3\mathbf{x}_1' d^3\mathbf{k}_1'}{(2\pi)^3} \frac{d^3\mathbf{x}_2' d^3\mathbf{k}_2'}{(2\pi)^3} W_q(\mathbf{x}_1', \mathbf{k}_1') W_{\bar{q}}(\mathbf{x}_2', \mathbf{k}_2') W_M(\mathbf{y}', \mathbf{k}'), \tag{4.14}$$

with the centroids of the quark and antiquark Winger functions situated at $(\mathbf{x}_1, \mathbf{k}_1)$ and $(\mathbf{x}_2, \mathbf{k}_2)$, respectively. In Eq.(4.13), we have taken into account the probability g_M for the color triplet, spin-$\frac{1}{2}$ quark and antiquark to form a color singlet meson of certain spin. We note that for a quark and antiquark pair of different masses m_1 and m_2, the relative coordinate and relative momentum in the meson Wigner function are defined by

$$\mathbf{y} = \mathbf{x}_1 - \mathbf{x}_2, \quad \mathbf{k} = \frac{1}{m_1 + m_2}(m_2\mathbf{k}_1 - m_1\mathbf{k}_2). \tag{4.15}$$

Similarly, the momentum spectrum of baryons from the recombination of three quarks is given by

$$\begin{aligned} \frac{dN_B}{d^3\mathbf{K}_B} = g_B \int & d^3\mathbf{x}_1 d^3\mathbf{k}_1 d^3\mathbf{x}_2 d^3\mathbf{k}_2 d^3\mathbf{x}_3 d^3\mathbf{k}_3 f_{q_1}(\mathbf{x}_1, \mathbf{k}_1) f_{q_2}(\mathbf{x}_2, \mathbf{k}_2) \\ & \times f_{q_3}(\mathbf{x}_3, \mathbf{k}_3) \overline{W}_B(\mathbf{y}_1, \mathbf{k}_1; \mathbf{y}_2, \mathbf{k}_2) \delta^{(3)}(\mathbf{K}_B - \mathbf{k}_1 - \mathbf{k}_2 - \mathbf{k}_3), \end{aligned} \tag{4.16}$$

where $\overline{W}_B(\mathbf{y}_1, \mathbf{k}_1; \mathbf{y}_2, \mathbf{k}_2)$ is the overlap integral of the baryon Wigner function with the quark Wigner functions, similar to Eq.(4.14) for the meson. While $\mathbf{y}_1$ and $\mathbf{k}_1$ in Eq.(4.16) are similarly defined as in Eq.(4.15), the second relative coordinate $\mathbf{y}_2$ and relative momentum $\mathbf{k}_2$ are given by

$$\begin{aligned} \mathbf{y}_2 &= \frac{m_1\mathbf{x}_1 + m_2\mathbf{x}_2}{m_1 + m_2} - \mathbf{x}_3, \\ \mathbf{k}_2 &= \frac{m_3(\mathbf{k}_1 + \mathbf{k}_2) - (m_1 + m_2)\mathbf{k}_3}{m_1 + m_2 + m_3}, \end{aligned} \tag{4.17}$$

respectively, with m_3 being the mass of the third quark (or antiquark). The factor g_B is the probability for three color triplet, spin-1/2 quarks (antiquarks) to form a color singlet baryon (antibarion) of certain spin.

In Ref. [14] for recombination of thermal partons among themselves and with jet partons, both the color and spin quantum numbers are treated on a purely statistical basis. The color flow in the parton shower is in principle tractable, although not yet implemented here for simplicity. Since the number of shower partons in a jet is very small, strong color correlations exist and the probability for colored shower partons to form color singlet hadrons is thus much larger than given by the statistical factor for colored thermal partons. For the present study, we will neglect the statistical factors due to the color degrees of freedom and only include those due to the spin degrees of freedom. However, we prohibit the quark-antiquark pair from a forced gluon decay to recombine into a color-singlet meson. This approximation can be justified by either invoking local color neutrality arguments [43, 49], as also used for cluster hadronization in HERWIG, or a color evaporation approach, similar to the one used in heavy quarkonium production in nuclear reactions where the quark and antiquark pair's wave function is assumed to be readjusted to a color singlet through soft gluon emission prior to form a bound state [50, 51, 52]. Of course this could be

improved in the future by following the color flow in the parton shower simulation.

In the present study, the phase-space distributions of quarks and antiquarks are obtained from the shower partons from the Monte Carlo jet shower generator. Taking the wave function of the shower parton as a Gaussian wave packet, $\exp[i\mathbf{k}_0\cdot\mathbf{x}-(\mathbf{x}-\mathbf{x}_0)^2/(2\delta^2)]$ with $\mathbf{x}_0$ and $\mathbf{k}_0$ denoting its coordinate and momentum, its Wigner function is then Gaussian in both coordinate and momentum spaces as shown in APPENDIX B. For the hadron wave functions, we take them to be those of harmonic oscillator potentials. In this case, their Wigner functions are also Gaussians in coordinate and momentum spaces. We can then evaluate Eq.(4.14) with the help of some mathematics worked out in APPENDIX B. The result for a meson in the n-th excited state in the center of mass frame of the quark-antiquark pair is

$$\overline{W}_{M,n}(\mathbf{y},\mathbf{k}) = \frac{v^n}{n!}e^{-v}. \tag{4.18}$$

with

$$v = \frac{1}{2}\left(\frac{\mathbf{y}^2}{\sigma_M^2}+\mathbf{k}^2\sigma_M^2\right). \tag{4.19}$$

where σ_M is the width of the harmonic oscillator wave function for the relative motion of the quark-antiquark pair.

Similarly, the overlap integral of the quark Wigner functions with the baryon Wigner function in the n_1-th excited state in one relative coordinate and in the n_2-th excited state in the other relative coordinate, is given by

$$\overline{W}_{B,n_1,n_2}(\mathbf{y}_1,\mathbf{k}_1;\mathbf{y}_2,\mathbf{k}_2) = \frac{v_1^{n_1}}{n_1!}e^{-v_1}\cdot\frac{v_2^{n_2}}{n_2!}e^{-v_2}, \tag{4.20}$$

with

$$v_i = \frac{1}{2}\left(\frac{\mathbf{y}_i^2}{\sigma_{Bi}^2} + \mathbf{k}_i^2\sigma_{Bi}^2\right), \quad i = 1, 2. \tag{4.21}$$

Since the wave functions of quarks and/or antiquarks in a hadron are always given in the rest frame of the hadron, we evaluate the relative coordinates and momenta in Eqs.(4.15) and (4.17) using the parton coordinates and momenta given at *constant rest frame time* [53, 54] in terms of their equal-time coordinates in the hadron rest frame. To this end, for each candidate partons to be treated their phase-space coordinates have to be Lorentz transformed from the lab frame to their common rest frame, and subsequently the partons produced earlier in the parton shower are propagated like free particles to the time at which the last candidate parton is produced and available for hadronization. We have checked that an algorithm that rather takes the distance of the closest approach for the candidate partons has not much influence on the results as the parton shower is rapidly expanding.

The two width parameters σ_{B1} and σ_{B2} in the baryon Wigner function are related to each other by

$$\sigma_{B2} = \sigma_{B1}\left(\frac{\mu_1}{\mu_2}\right)^{1/2}, \tag{4.22}$$

where the two reduced masses are defined as [55]

$$\mu_1 = \frac{m_1 m_2}{m_1 + m_2}, \quad \mu_2 = \frac{(m_1 + m_2)m_3}{m_1 + m_2 + m_3}. \tag{4.23}$$

The width parameters in the hadron Wigner functions can be related to the measured size of the formed hadron. More precisely, for a meson consisting of quark and antiquark of masses m_1 and m_2 and quark charges Q_1 and Q_2, its mean-square

charge radius is related to σ_M by [55]

$$\langle r^2\rangle_M = |\langle Q_1(\mathbf{x}_1-\mathbf{X})^2+Q_2(\mathbf{x}_2-\mathbf{X})^2\rangle| = \frac{3}{2}\frac{|Q_1m_2^2+Q_2m_1^2|}{(m_1+m_2)^2}\sigma_M^2, \quad (4.24)$$

where $\mathbf{X}=(m_1\mathbf{x}_1+m_2\mathbf{x}_2)/(m_1+m_2)$ is the center of mass coordinate.

Similarly, the width parameter σ_{B1} in the Wigner function of a baryon consisting of three quarks of masses m_1, m_2, and m_3, and charges Q_1, Q_2, and Q_3 are related to its mean-square charge radius is by [56]

$$\begin{aligned}\langle r^2\rangle_B &= |\langle Q_1(\mathbf{x}_1-\mathbf{X})^2+Q_2(\mathbf{x}_2-\mathbf{X})^2+Q_3(\mathbf{x}_3-\mathbf{X})^2\rangle| \\ &= \frac{3\sigma_{B1}^2}{2(m_1+m_2+m_3)}\Big[\frac{m_2(m_2+m_3)}{m_1+m_2}Q_1+\frac{m_1(m_3+m_1)}{m_1+m_2}Q_2+\frac{m_1+m_2}{m_3}Q_3\Big],\end{aligned} \quad (4.25)$$

where $\mathbf{X}=(m_1\mathbf{x}_1+m_2\mathbf{x}_2+m_3\mathbf{x}_3)/(m_1+m_2+m_3)$ denotes the center of mass of the three quarks.

Table 4.1: Empirical charge radii R_c (from Ref. [10]), width parameters σ_M or σ_{B1}, and spin statistical factors g for hadrons used in the calculation. Table adapted from Ref. [3].

Hadron	R_c [fm]	σ_M or σ_{B1} [fm]	g
π	0.67	1.09	1/4
ρ	–	1.09	3/4
K	0.56	0.84	1/4
K^*	–	0.84	3/4
N	0.88	1.24	1/4
N^*	–	1.24	1/4
Δ	–	1.24	1/2
Λ	–	1.21	1/4

We use measured charge radii for charged pions, protons and charged kaons to determine the width parameters σ_π, σ_K and σ_N in the pion, kaon and nucleon Wigner functions. The same width parameters are used for their isospin partners and their antiparticles as well as their spin resonances ρ, K^*, N^*, and Δ. Since Λ and $\bar{\Lambda}$ have no charge, their width parameters are determined instead from the matter radius, which is given by an equation similar to Eq. (4.25) after setting $Q_1 = Q_2 = Q_3 = 1/3$, and assuming that their size is the same as that of a proton. Excited states of these hadrons are then accounted for by the excited states of the harmonic oscillator wave functions using the same width parameters. In Table I, we summarize the charge radii, width parameters and spin statistical factors for all stable hadrons and resonances included here.

Eqs. (4.18) and (4.20) can now be used to determine the recombination probability for a given quark-antiquark pair or a triplet of quarks or antiquarks. For a given shower, the relative coordinates in the common rest frame are evaluated for all possible hadron candidates which are subsequently accepted for recombination, or rejected, by Monte Carlo methods.

Some quarks might have quite small probabilities for recombination with any other parton in the same shower. In that case, there is a large probability that the Monte Carlo algorithm will not find a recombination partner. Such quarks are typically far removed from others in phase space, making all Wigner function overlap integrals small. The reason for this to occur is the lack of confinement in what is essentially a perturbative shower evolution. Of course isolated partons have to be connected by strings to another color charge and Lund string fragmentation can take care of their hadronization. We deal with such partons far removed in phase space by reconnecting them to other partons by QCD strings. This also includes undoing the non-perturbative gluon splitting introduced earlier, if none of the daughter quarks

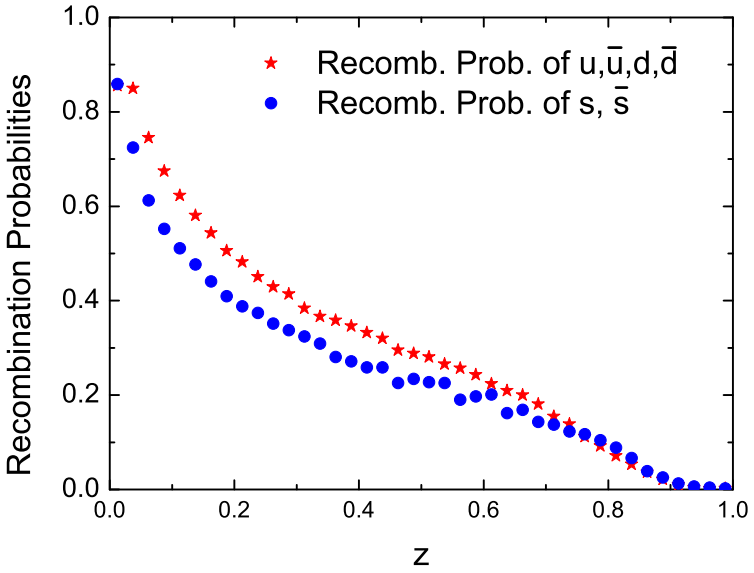

Figure 4.3: Probabilities of light and strange quarks to recombine into hadrons as functions of their momentum fraction z for 100 GeV jets. Figure adapted from Ref. [3].

has found a recombination partner. We thus form short strings of the types $(q, \bar{q})$, $(q, g, g, \ldots, \bar{q})$, (q, qq), and $(q, g, g, \ldots, qq)$, where q, g, $\bar{q}$, and qq denote quark, gluon, antiquark, and diquark, respectively, and then hand them over to PYTHIA 6.3 for hadronization by using a subroutine PYEXEC.

We end up with the following picture: Final hadron spectra are a mixture of hadrons from recombination (from quarks close in phase space to other quarks) and from string fragmentation (for quarks isolated in phase space or otherwise leftover). Typically, high-z partons are both rare and far removed in phase space. They are unlikely to recombine with other partons in the shower (or partons from a surrounding medium if one would consider such). This can be seen in Fig. 4.3 where the probability of quarks to find a recombination partner is plotted as a function of

parton momentum fraction z for 100 GeV jets. Thus in our model moderate to high-z partons still preferentially hadronize by string breaking. On the other hand, we indeed find the existence of a bulk of jet partons at lower z in which quarks are close enough in phase space so that they prefer recombination. Recall that our main motivation is to establish a hadronization model which naturally generalizes to jets in a medium. It is now straightforward to see how our formalism can be applied to that more general case, which will be described in Section 6.

Excited states are important channels for recombination. Excited mesons and baryons up to $n = 5$ are known experimentally [10]. However, we include contributions from excited meson states up to $n = 8$ and excited baryon states up to $n_1 + n_2 = 8$, which can be easily done with harmonic oscillator wave functions. We allow excited states to decay to multiple pions in the case of light quark mesons, to kaon and pion in the case of light and strange mesons, to (anti)nucleon and pion in the case of light quark (anti)baryons, and to Λ and pion in the case of light and strange quark (anti)baryons. For decays into multiple pions, we determine their relative probabilities through the available phase space according to [57]

$$P_l(M) \sim \left[\frac{1}{6\pi^2}\left(\frac{M}{m_\pi}\right)^3\right]^l \frac{(4l-4)!(2l-1)}{(2l-1)!^2(3l-4)!}\,. \tag{4.26}$$

Here l is the number of pions, M is the mass of the excited state, or the invariant mass of the light quark-antiquark pair. The pion mass m_π in the above equation comes from taking the radius of the emitting source to be that of the inverse of the pion mass [57]. In the present study, we replace $1/m_\pi$ by the distance between the recombined quark and antiquark, and consider its decay to at most four pions. The momentum distribution of these pions is then determined from phase space considerations. An excited nucleon N^* or Δ decays to a nucleon and l pions if its

invariant mass is between $m_N + lm_\pi$ and $m_N + (l+1)m_\pi$ with m_N being the nucleon masses. Again, we include at most four pions in the decay and use phase space considerations to determine their momenta. An excited kaon or Λ is assumed to decay to a kaon or Λ and multi-pions in a similar way. Details on the phase space calculations are described in APPENDIX C.

4.3 Results

In the following, we compare our results for hadrons obtained recombination of the parton showers from PYTHIA to the calculation in PYTHIA with string fragmentation obtained with the same parton showers.

First, we have tested the longitudinal structure of jets by comparing the spectra dN/dz as functions of the momentum fraction z longitudinal to the jet axis for our sample of 100 GeV jets. In Fig. 4.4, we show the spectra of pions (upper left panel), kaons (upper right panel), nucleons and antinucleons (lower left panel), and Λ and $\bar{\Lambda}$ (lower right panel) from 100 GeV quark jets. We show separately hadrons from recombined shower partons (stars), from the fragmentation of remnant hadrons (circles) and their sum (dashed line). The solid line indicates the result from PYTHIA 6.3 string fragmentation applied to the same sample of jet parton showers. We also show the recombination only through the ground state of the harmonic oscillator wave functions ($n = 0$). As expected, we see that recombination spectra fall off faster with z than the string fragmentation contribution. String fragmentation dominates at intermediate and high z while recombination becomes the leading channel below $z \sim 0.1$, where the bulk of the hadron production resides.

We also note that recombination proceeds mainly through excited hadron states and not directly into $n = 0$ ground state hadrons. The $n = 0$ channel includes direct production of pion, kaon, nucleon, and Λ as well as production from the decay of $n =$

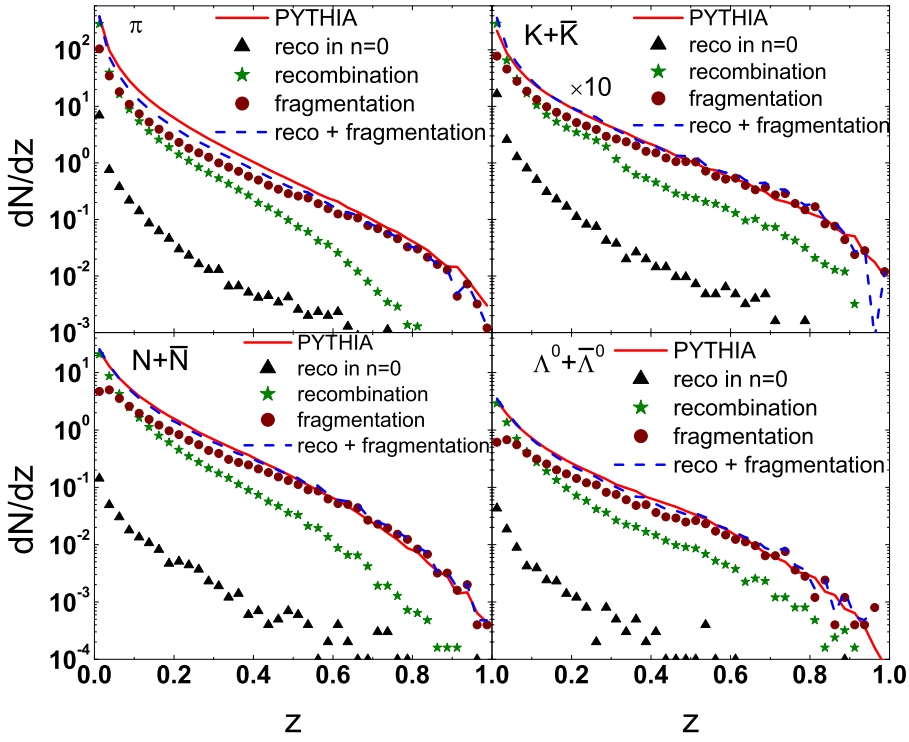

Figure 4.4: Spectrum dN/dz of pions (upper left panel), kaons (upper right panel), nucleons and antinucleons (lower left panel), and Λ and $\bar{\Lambda}$ (lower right panel) from our calculation. Shown separately are contributions from the recombination of shower partons (stars) and fragmentation of remnant partons (circles). Also shown are the total contribution (dashed lines) and the results from PYTHIA string fragmentation (solid lines). Figures adapted from Ref. [3].

0 spin-excited states ρ, K^*, N^* and Δ. The inclusion of excited states $n > 0$ makes the recombination spectra considerably harder. Overall we find that our results are consistent with the spectra from PYTHIA based on the string fragmentation of all shower partons. Note that the comparison to string fragmentation — another model — only makes sense on a qualitative level. Precision tuning of our model would have to involve fits to data which is outside the scope of this work. We compare the transverse momentum spectra of jets in Fig. 4.5. Again, results obtained from our hybrid recombination and fragmentation model compare well to pure string

fragmentation.

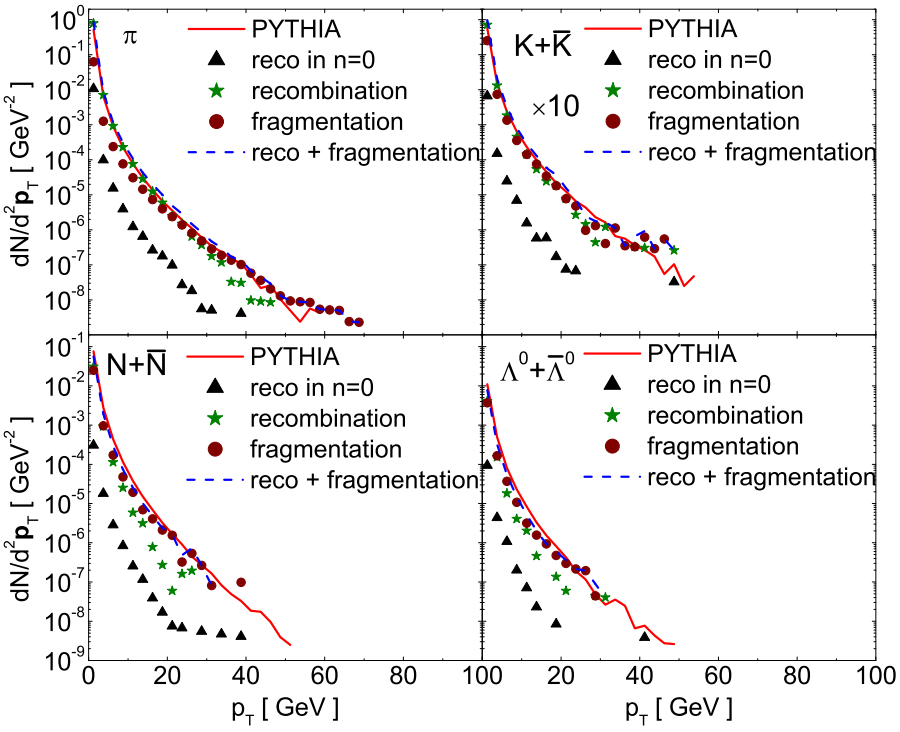

Figure 4.5: Same as Fig. 4.4 for the transverse momentum spectra. Figure adapted from Ref. [3].

Finally, we have checked our approach to hadronization with jets of a smaller jet energy and find again that our results reproduce pure string fragmentation reasonably well. The spectra for $E_{\rm jet} = 25$ GeV jets are shown in Figs. 4.6 and 4.7 for the longitudinal and transverse momentum spectra, respectively. The recombination probability depends on the absolute distance of partons in phase space. Hence we expect the range in z in which recombination competes with remnant string fragmentation to decrease with rising $E_{\rm jet}$. On the other hand, at smaller jet energies

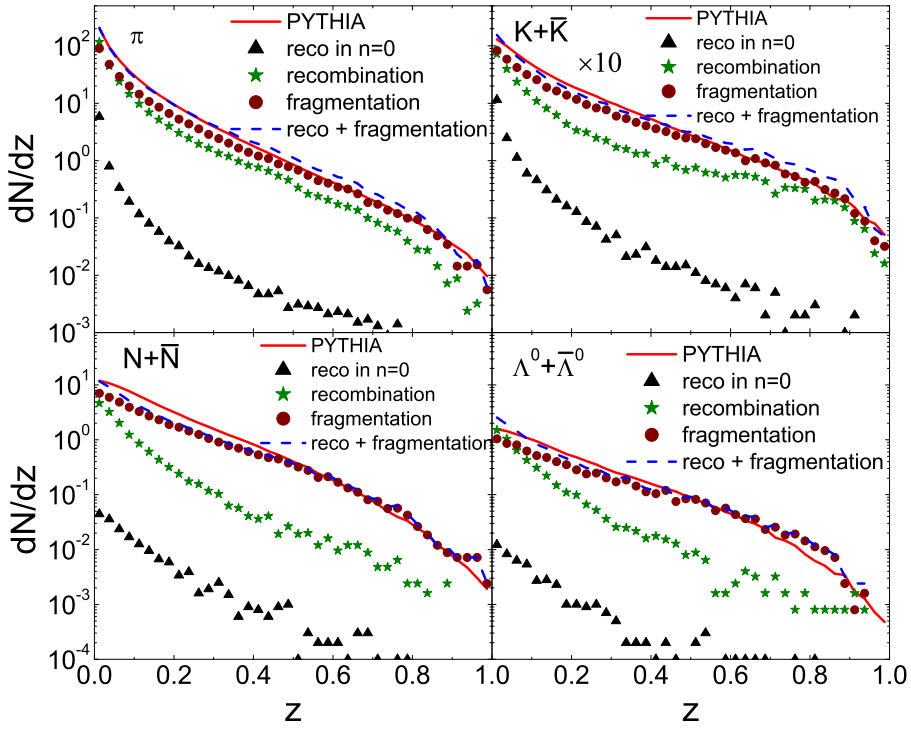

Figure 4.6: Same as Fig. 4.4 for jets of energy $E_{\rm jet} = 25$ GeV. Figure adapted from Ref. [3].

recombination stays more competitive out to larger z at least for mesons, while for baryons the reduced number of partons in lower energy jets can lead to the opposite effect.

4.4 Summary

We have devised a model to hadronize perturbative parton showers in jets based on a hybrid of quark recombination and string fragmentation. Our algorithm reproduces results from pure string fragmentation and can be easily generalized to include partons from an ambient medium.

We have turned perturbative parton showers into showers of constituent quarks and antiquarks by gluon decay. We then apply Monte Carlo methods to recom-

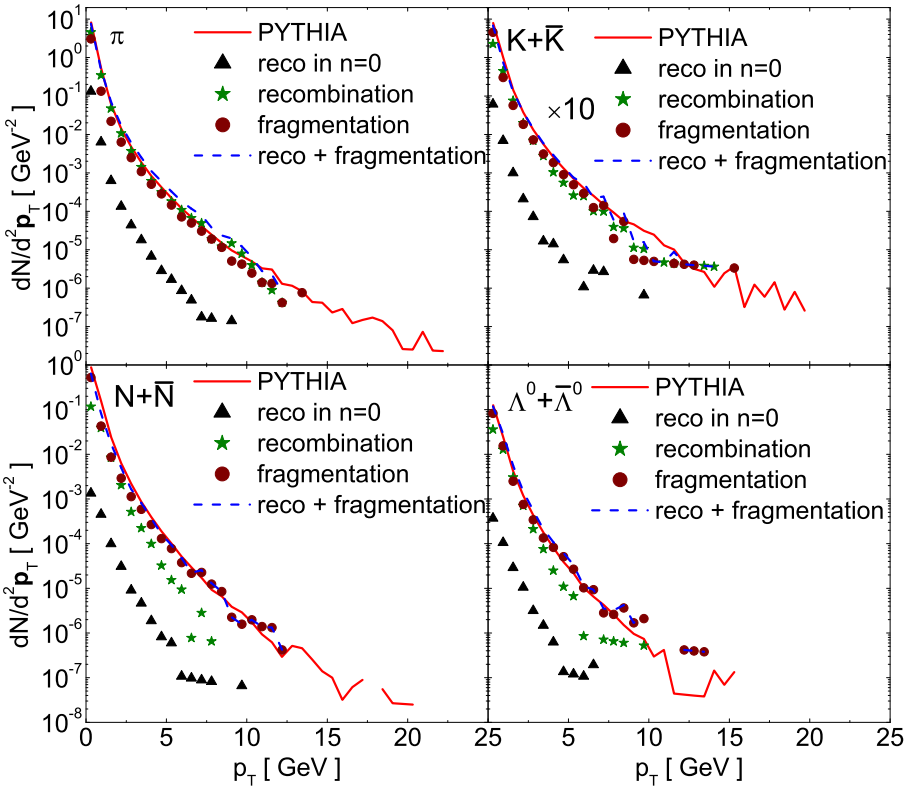

Figure 4.7: Same as Fig. 4.5 for jets of energy $E_{\rm jet} = 25$ GeV. Figure adapted from Ref. [3].

bine quarks and antiquarks using probabilities given by the overlap integrals of their Wigner functions with the meson and baryon Wigner functions. The width parameters in these Wigner functions are fixed by hadron charge radii. Remnant quarks and antiquarks, which are not used for recombination, are connected by strings and subjected to the usual string fragmentation procedure in PYTHIA. We have found that decays of excited states from recombination make the most important contributions to spectra of pions, kaons and nucleons.

We have checked that both the longitudinal and transverse momentum structures of hadron showers reproduce the results from PYTHIA string fragmentation. The

only adjustable parameter that we have kept is the mass cutoff for gluon decays into quark-antiquark pair which can be set by the strange to non-strange hadron ratio. However, other quantities which are not very well known, like the width parameters in the Wigner functions for excited states of hadrons, can in principle be used as parameters for further fine tuning of results.

Our hybrid approach essentially keeps string dynamics intact for the high-z tail of the jet and replaces string dynamics with recombination for the bulk of the jet where $\mathcal{O}(10)$ quarks with a few GeV/c momentum can be found close enough together in phase space to recombine.

In the presence of a quark-gluon plasma produced in relativistic heavy ion collisions, our approach can be generalized by sampling the ambient medium (e.g. provided by a fluid dynamic simulation into which the jet is embedded) for thermal partons. Recombination would be delayed if the ambient temperature is above the critical temperature T_c. At T_c jet partons would be allowed to recombine with thermal partons, and remnant jet partons could also be allowed to connect to thermal partons by strings. This process, like other jet-medium interactions, would allow the exchange of energy and momentum. Details of an in-medium algorithm is provided in Section 6.

5. JET QUENCHING IN HEAVY ION COLLISIONS

5.1 Energy Loss of Jet partons

Jets created from hard scattering in heavy ion collisions can interact with the medium partons in QGP and lose some of their energies. Energy losses of jet partons are caused by their elastic and inelastic scattering in the medium. These are called the collisional and the radiative energy loss because the former is caused by the quasi-scattering between jet partons and medium partons, and the latter by the gluon radiation induced by the inelastic scattering of jet partons in medium.

Bjorken pioneered in calculating the collisional energy loss [58] and obtained

$$-\frac{dE}{dx} = C_{\mathrm{R}}\pi\alpha_s^2\left(1+\frac{N_{\mathrm{f}}}{6}\right)\ln\frac{4ET}{m_D^2}, \tag{5.1}$$

where the Debye screening mass in a QCD plasma is given by $m_D = \left(1+\frac{N_{\mathrm{f}}}{6}\right)g^2T^2$. Several studies on energy loss caused by elastic collisions of partons in a medium were subsequently performed by others [59, 60, 61].

Further studies [62, 63] showed that gluon bremsstrahlung induced by multiple scattering of a jet parton in QGP played a more significant role in the energy loss of the jet. Several phenomenological models for calculating the radiative energy loss were introduced in the literatures, which can be divided into following four categories: (1) *Multiple soft scattering*: In the BDMPS-Z [64, 65] and ASW [66, 67, 68] models, it is assumed that the medium can be modeled by a series of static colored scattering centers, whose densities decrease with its expansion. The medium is specified by the transport coefficient $\hat{q}$, which is the mean of the squared transverse momentum exchanged between the jet parton and the medium per unit path length.

(2) *Opacity expansion*: In the GLV [63, 69, 70, 71, 72] model, as in the BDMPS-Z, the medium is assumed to be a series of static scattering centers, but the energy loss is determined by an expansion in the opacity $\bar{n} = L/\lambda$ with L and λ denoting the path length and mean free path, respectively, which is the number of the scatterings between the jet and medium partons.

(3) *Higher twist (HT)*: In this model [73, 74, 75], the medium is formulated in terms of matrix elements of gauge field operators and is characterized by its entropy density s.

(4) *Finite temperature field theory*: In the AMY [76, 77, 78, 79, 80] model, the medium is characterized as a thermally equilibrated plasma, which is specified by its temperature T and baryon chemical potential μ_B. This approach is formulated in the finite temperature field theory using the Hard Thermal Loop approximation.

All approaches enumerated above are based on the QCD factorization expressed by

$$d\sigma_{AB\to h} = f_{a/A}(x_1, Q^2) \otimes f_{b/B}(x_2, Q^2) \otimes d\sigma_{ab\to c}(x_1, x_2, Q^2) \otimes D_{c\to h}(z, Q^2), \quad (5.2)$$

where $f_{a/A}(x_1, Q^2)$ and $f_{b/B}(x_2, Q^2)$ are the parton distribution function (PDF) of nucleon a in nucleus A and that of b in B, respectively, the momentum fractions x_1 and x_2 are given by $x_1 \equiv p_a/p_A$ and $x_2 \equiv p_b/p_B$, $d\sigma_{ab\to c}(x_1, x_2, Q^2)$ is the inclusive differential cross section for the hard process $ab \to c$ in the partonic level, and $D_{c\to h}(z, Q^2)$ is the fragmentation function (FF) that gives the probability for parton c to fragment into the observed hadron h with fractional momentum z. $d\sigma_{ab\to c}$ can be calculated by the perturbative QCD while the FF and the PDFs are obtained from the experimental results. To take into account the in-medium effect due to energy loss, FF is modified as $D^{\rm vac}_{c\to h}(z) \to D^{\rm med}_{c\to h}(z', \hat{q})$ during hadronization, where $z'(< z)$

and $\hat{q}$ encode the information about the parton energy loss. The final hadronization process from hard partons to the observed hadrons is assumed to occur in the vacuum after partons have traversed through the QGP.

To study medium modificatoin of jet fragmentation, we use the approach developed in the last decade and described in Refs. [67, 81, 82, 83, 84] to take into account the effect of shower parton energy loss. Using the lowest-order (LO) perturbative QCD, the inclusive high-p_T hadron cross section [85] in $A+A$ collisions can be calculated according to

$$\begin{aligned}\frac{d\sigma^h_{AA}}{dyd^2\mathbf{p}_T} &= K\sum_{abcd}\int d^2\mathbf{b}d^2\mathbf{r}dx_a dx_b d^2\mathbf{k}_{aT}d^2\mathbf{k}_{bT}t_A(r)t_A(|\mathbf{b}-\mathbf{r}|)\mathrm{g}_A(k_{aT},r)\\ &\times \mathrm{g}_A(k_{bT},|\mathbf{b}-\mathbf{r}|)f_{a/A}(x_a,Q^2,r)f_{b/A}(x_b,Q^2,|\mathbf{b}-\mathbf{r}|)\\ &\times \frac{D_{h/c}(z_c,Q^2,\Delta E_c)}{\pi z_c}\frac{d\sigma}{d\hat{t}}(ab\to cd),\end{aligned} \tag{5.3}$$

where $z_c = p_T/p_c$, $y = y_c$, $\sigma(ab \to cd)$ denotes the cross section of the elementary parton scattering, and $t_A(b)$ is the nuclear thickness function with the normalization $\int d^2bt_A(b) = A$. In this approach, the hard-sphere model of nuclear distribution is used and the factor $K \approx 1.3-2$ encodes higher-order perturbative QCD corrections. The following assumptions are then introduced: (1) The parton distribution per nucleon $f_{a/A}(x_a, Q^2, r)$ inside a nucleus can be factorized into the parton distributions in a free nucleon given by the MRSD-' parametrization [86] and the impact parameter dependent nuclear modification factor [87, 88]. (2) The initial transverse momentum distribution $\mathrm{g}_A(k_T, Q^2, b)$ has a Gaussian form with a width that includes effects from both the intrinsic motion in the nucleon and the nuclear broadening [84]. The

medium modification of FF's can be well approximated by [67, 89, 73]

$$\begin{aligned} D_{h/c}(z_c, Q^2, \Delta E_c) &= (1 - e^{-\langle \frac{\Delta L}{\lambda} \rangle}) \Big[\frac{z_c'}{z_c} D^0_{h/c}(z_c', Q^2) + \Big\langle \frac{\Delta L}{\lambda} \Big\rangle \frac{z_{\rm g}'}{z_c} D^0_{h/{\rm g}}(z_{\rm g}', Q^2) \Big] \\ &+ e^{-\langle \frac{\Delta L}{\lambda} \rangle} D^0_{h/c}(z_c, Q^2), \end{aligned} \tag{5.4}$$

where $z_c' = p_T/(p_{Tc} - \Delta E_c)$ and $z_{\rm g}' = \langle \Delta L/\lambda \rangle p_T/\Delta E_c$ are the rescaled momentum fractions and ΔE_c denotes the total parton energy loss during the number of scatterings $\langle \Delta L/\lambda \rangle$. The FF in free space $D^0_{h/c}(z_c, Q^2)$ are given by the BKK independent fragmentation [90]. The gluon density $\rho_{\rm g}(\tau, r)$ of the expanding medium is assumed to be proportional to the transverse profile of the participant nucleons. The average number of scatterings along the path is written as

$$\Big\langle \frac{\Delta L}{\lambda} \Big\rangle = \int_{\tau_0}^{\tau_0 + \Delta L} d\tau \sigma \rho_{\rm g}(\tau, b, \mathbf{r} + \mathbf{n}\tau), \tag{5.5}$$

where $\Delta L(b, \mathbf{r}, \phi)$ is the distance traversed by a jet created at $\mathbf{r}$ along $\mathbf{n}$ at an azimuthal angle ϕ with respect to the reaction plane in a collision with impact parameter b.

In Refs. [67, 81, 89], it has been shown that the total parton energy loss in a finite and expanding medium is given by a path integral,

$$\Delta E = \Big\langle \frac{dE}{dL} \Big\rangle_{\rm 1D} \int_{\tau_0}^{\infty} d\tau \left(\frac{\tau - \tau_0}{\tau_0} \right)^{\alpha} \frac{\rho(\tau, \mathbf{r})}{\rho(\tau_0, 0)} \frac{p^\mu u_\mu}{p^0}, \tag{5.6}$$

for a parton produced at a transverse position $\mathbf{r}$ and moving along the jet path. In the above, α is the parameter for specifying the path-length dependence of jet energy loss with possible values of 0, 1, 2; p^μ and u_μ are, respectively, the four-momentum of the jet and the four-velocity of the flow of local medium; and $\left\langle \frac{dE}{dL} \right\rangle_{\rm 1D}$ is the average

parton energy loss per unit length in a 1D expanding medium. For $\left\langle \frac{dE}{dL} \right\rangle_{\rm 1D}$, we use the numerical results obtained in Refs. [82, 89] that include the effect of thermal gluon absorption, i.e.,

$$\left\langle \frac{dE}{dL} \right\rangle_{\rm 1D} = \epsilon_0 (E/\mu_0 - 1.6)^{1.2}/(7.5 + E/\mu_0), \tag{5.7}$$

where ϵ_0 is the energy loss parameter with a value that is 9/4 times larger for a gluon than for a quark, and the Debye mass μ_0 is given by $\mu_0 = 1.5$ GeV [70].

5.2 Jet Quenching in Heavy Ion Collisions

In the previous section, we have described several ways on how to find the energy loss of partons traversing through the medium without comparing with experimental measurements. Experimental measurement of jet quenching includes mainly two measurements. One is the single hadron spectrum which was found to be significantly suppressed at high-p_T in central collisions [6, 44, 91, 92]. Another is the azimuthal correlation in the angular distribution of dihadron that was found to be strongly modified in central A+A collisions compared to that from pp collisions [93, 94]. The former provides an inclusive measurement of the total effect of the suppression on the p_T-spectrum while the latter gives a differential measurement of the quenching as it is sensitive to the quenching of one jet with respect to the other jet.

For quantifying the amount of suppression, the nuclear modification factor defined as

$$R_{\rm AA} = \frac{1}{N_{\rm coll}^{\rm AA}} \frac{dN^{\rm AA}/dyd^2\mathbf{p}_\perp}{dN^{pp}/dyd^2\mathbf{p}_\perp}, \tag{5.8}$$

has been introduced, where $dN^{\rm AA}/dyd^2\mathbf{p}_\perp$ and $dN^{pp}/dyd^2\mathbf{p}_\perp$ are, respectively, the differential hadron yields in A+A and $p+p$ collisions, and $N_{\rm coll}^{\rm AA}$ is the number of

binary nucleon-nucleon collisions in a nucleus-nucleus collision. Experimental results on the R_{AA} from both PHENIX and STAR have shown that the production of high transverse momentum particles is strongly influenced by the medium produced in heavy ion collisions.

6. MEDIUM MODIFICATION OF JET FRAGMENTATION IN HEAVY ION COLLISIONS

In Section 4, we have reproduced jet fragmentation by recombining parton showers inside jets. As we stated briefly in 2.2, hadronization of energetic jets produced in heavy ion collisions has been usually described by using fragmentation functions, which are parameterized using experimental data from elementary collisions [12, 13]. However, it has been found that these fragmentation functions do not describe hadrons of intermediate transverse momenta in heavy ion collisions. On the other hand, it has been shown that the data can be understood in the coalescence model. In particular, the enhancement of the transverse momentum spectra of hadrons in the intermediate momentum region can be obtained from the coalescence of soft partons in the QGP and hard partons in minijets. Since jets evolve into shower partons, it is more appropriate to recombine thermal partons with shower partons in the jets instead of with the jets. This was included in Ref. [16]. However, the distribution of shower partons in this study was obtained from fitting the experimental data. Moreover, the recombination was carried out with partons from mixed events.

In this section, we study the transverse momentum spectra of hadrons produced in central heavy ion collisions by including the medium modification of jet fragmentation via the parton coalescence. We carry out this study by applying recombinations to both thermal partons in the QGP and parton showers inside the jets produced in heavy-ion collisions. We use the Monte Carlo method to generate thermal partons in QGP based on a blast-wave model. For the shower partons in jets, they are obtained from the branching of jets of power law p_T spectra from PYSHOW, a subroutine in

PYTHIA [22]. Thermal partons can then allowed to recombine among themselves and also with shower partons to form hadrons. For the recombination of shower partons among themselves, the same method as in the previous section is used to form hadrons. Shower partons that remain after recombinations among themselves will form strings to fragment into hadrons, which will be calculated by using the subroutine PYEXEC in PYTHIA. These studies are carried out for central Au+Au collisions at $\sqrt{s_{NN}} = 200$ GeV available at RHIC and central Pb+Pb collisions at $\sqrt{s_{NN}} = 2.76$ TeV available at LHC. While jets produced in heavy-ion collisions traversing through QGP, their energies are reduced due to the interaction with thermal partons in the medium. Assuming that a jet traversing through medium loses a certain amount of its energy before each branching and using the formula introduced in Ref. [19], we obtain shower partons after taking into account of the energy losses of the jets. We then recombine quenched shower partons with thermal partons as well as among themselves to study hadron spectra. We further compare our results with those from experimental measurements conducted at RHIC and LHC.

6.1 Thermal Partons in QGP and Parton Showers inside Jets in Heavy Ion Collisions

In our study, partons are classified into two components: thermal partons in QGP and shower partons inside jets. The former are dominant at the low momentum region, and their transverse momentum distribution has an exponential form. The latter are dominant at the high momentum region and their transverse momentum spectra have power law distributions. In the present study, we consider central Au+Au collisions (0-10 %) at $\sqrt{s_{NN}} = 200$ GeV at RHIC and central Pb+Pb collisions (0-5 %) at $\sqrt{s_{NN}} = 2.76$ TeV at LHC.

We first generate thermal partons in the produced QGP by using the blast wave

model. In the mid-rapidity region $|y| < 0.5$, the longitudinal momenta of the thermal partons are assumed to be given by the boost-invariant distribution, i.e. uniform in y, while the transverse momentum spectra of these partons have an exponential form given by [11]

$$\frac{dN_{q,\bar{q}}}{d^2\mathbf{r}_T d^2\mathbf{p}_T} = \frac{g_{q,\bar{q}}\tau m_T}{(2\pi)^3} \exp\Big(- \frac{\gamma_T(m_T - \mathbf{p}_T \cdot \mathbf{v}_T) \mp \mu_b}{T}\Big). \tag{6.1}$$

In the above equation, the spin-color degeneracies of partons $g_{q,\bar{q}}$ are 6 for quark and anti-quark and 16 for gluon. According to the blast wave model, the flow velocity v_T depends on the collective flow velocity β and transverse radial position of partons by $\mathbf{v}_T = \beta(\mathbf{r}_T/R_\perp)$, where $R_\perp$ denotes the radial size of the QGP at proper time τ_c. The spatial distribution of thermal partons in the transverse direction are taken to be isotropic. Their longitudinal coordinates and times are, on the other hand, determined by $z = \tau_c \sinh y$ and $t = \tau_c \cosh y$ as we have assumed the Bjorken correlation $\eta = y$ [95]. The temperature in the QGP is taken to be $T = 170$ MeV and μ_b is the baryon chemical potential. The transverse momentum spectra for strange quarks have similar forms as Eq. (6.1) but without $\mp\mu_b$ because the numbers of strange and antistrange quarks are the same. The parameters used for the fireball in central (0-10%) Au+Au collisions at $\sqrt{s_{NN}} = 200$ GeV and in the central (0-5%) Pb+Pb collisions at $\sqrt{s_{NN}} = 2.76$ TeV are shown in Table 6.1. Furthermore, we take $m_{q,\bar{q}} = m_g = 330$ MeV for the masses of light quarks and gluons and $m_{s,\bar{s}} = 500$ MeV for that of strange quarks in the QGP. Although the transverse shape of the QGP is not quite isotropic, according to the finite elliptic flow of hadrons measured in experiments, we neglect this effect because we are interested in results that are integrated over all azimuthal angles. The numbers of quarks per unit of rapidity in

Table 6.1: The fireball parameters used for thermal partons produced in central Au+Au collisions at $\sqrt{s_{NN}} = 200$ GeV [11] available at RHIC and in central Pb+Pb collisions at $\sqrt{s_{NN}} = 2.76$ TeV available at LHC.

	$R_\perp$ (fm)	τ (fm/c)	β (c)	T (MeV)	μ_b (MeV)
RHIC	8.3	4	0.5	170	10
LHC	12	6	0.65	170	0

the fireball are about $N_{u,d} \sim 258$, $N_{\bar{u},\bar{d}} \sim 241$, and $N_{s,\bar{s}} \sim 188$ at RHIC and about $N_{u,d,\bar{u},\bar{d}} \sim 620$ and $N_{s,\bar{s}} \sim 380$ at LHC.

Before generating parton showers in jets produced in heavy ion collisions, we first obtain the transverse momentum spectra of initial jets at midrapidity ($|y| \leq 0.5$) by multiplying those from $p + p$ collisions at the same energies in PYTHIA with the number of binary collisions about 960 in central (0-10%) Au+Au collisions at $\sqrt{s_{NN}} = 200$ GeV and about 1685 in central (0-5%) Pb+Pb collisions at $\sqrt{s_{NN}} = 2.76$ TeV, respectively. After fitting these transverse momentum spectra with a power law given by [11]

$$\frac{dN_{\rm jet}}{d^2\mathbf{p}_T} = A\Big(\frac{B}{B + p_T}\Big)^n, \tag{6.2}$$

we obtain the fitting parameters given in Table 6.2. The corresponding transverse momentum spectra of gluon (left panel), light quarks (middle panel), and strange quarks (right panel) for central Au+Au collisions at $\sqrt{s_{NN}} = 200$ GeV (top) and central Pb+Pb collisions at $\sqrt{s_{NN}} = 2.76$ TeV (bottom) are shown in Fig. 6.1.

The transverse momentum spectra of jets shown in Fig. 6.1 correspond to those produced in vacuum. When jets traverse through QGP, they lose some of their energies due to interactions with the medium partons and also due to the emission

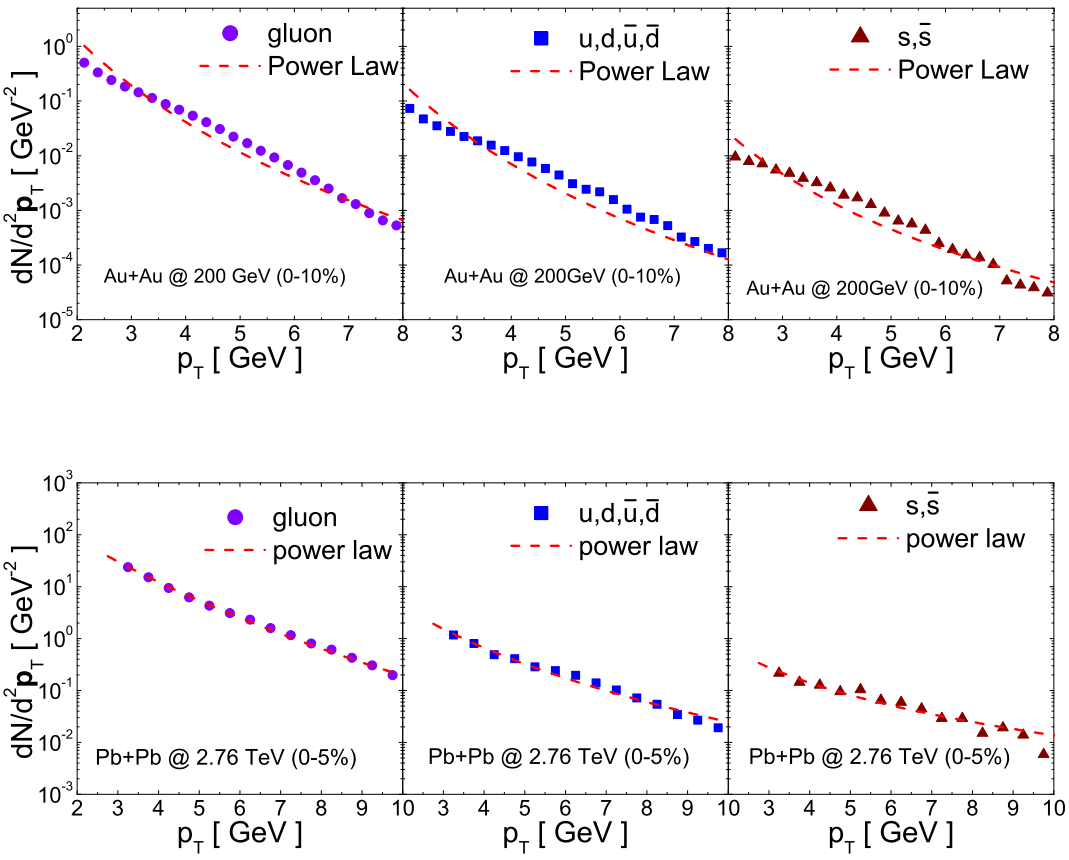

Figure 6.1: Transverse momentum spectra of gluon (left panels), light (middle panels) and strange quark (right panels) jets in central Au+Au collisions at $\sqrt{s_{NN}} = 200$ GeV (upper window) and Pb+Pb collisions at $\sqrt{s_{NN}} = 2.76$ TeV (lower window) obtained by multiplying those from p+p central collisions at the same energy in PYTHIA by the number of binary collisions.

of gluons.

We use the model described in Section 5 to calculate the energy loss. Assuming the medium to be uniform and taking $\alpha = 1$ in Eq. (5.6), the energy loss of the shower parton during splitting is then given by

$$\Delta E_{\rm shower} = \left\langle \frac{dE}{dL} \right\rangle_{1D} \frac{(\tau_{\rm cr} - \tau_{\rm sp})^2}{\tau_0} \frac{p^\mu u_\mu}{p^0} \tag{6.3}$$

Table 6.2: Parameters for transverse momentum distributions of jet partons in Eq. (6.2) at midrapidity from central Au+Au collisions at $\sqrt{s_{NN}} = 200$ GeV and from central Pb+Pb collisions at $\sqrt{s_{NN}} = 2.76$ TeV.

	RHIC			LHC		
	A (GeV^{-2})	B (GeV)	n	A (GeV^{-2})	B (GeV)	n
g	1500	1.23	7.27	90.0	7.10	9.60
$u, \bar{u}, d, \bar{d}$	210.0	1.2	7.04	7.28	2.65	5.11
$s, \bar{s}$	125.6	0.473	5.12	3.11	0.70	2.83

where $\tau_{\rm cr}$ and $\tau_{\rm sp}$ indicate the times when a shower parton is created and splits, respectively, and the time of the initial thermalization is taken to be $\tau_0 = 0.6$ fm/c. We then use Eq. (5.7) to find the average energy loss per unit length $\langle dE/dL \rangle_{\rm 1D}$. The values of ϵ_0 are determined from fitting the nuclear modification factor R_{AA} of pions obtained from our approaches to the hadronization with the experimental results at transverse momenta around 8 GeV. From the calculations described in the rest of this section, we have found the values of ϵ_0 are 3.5 GeV/fm for RHIC and 5.3 GeV/fm for LHC. In calculating R_{AA}, we divide the hadron spectra obtained from quenched shower partons by those from unquenched ones generated from the initial jets by using PYTHIA without energy loss.

In our calculations, we use PYTHIA to obtain shower partons inside jets that are produced in central Au+Au collisions at $\sqrt{s_{NN}} = 200$ GeV and in central Pb+Pb collisions at $\sqrt{s_{NN}} = 2.76$ TeV. Before each branching, shower partons lose energies according to the formula given in Eq. (6.3).

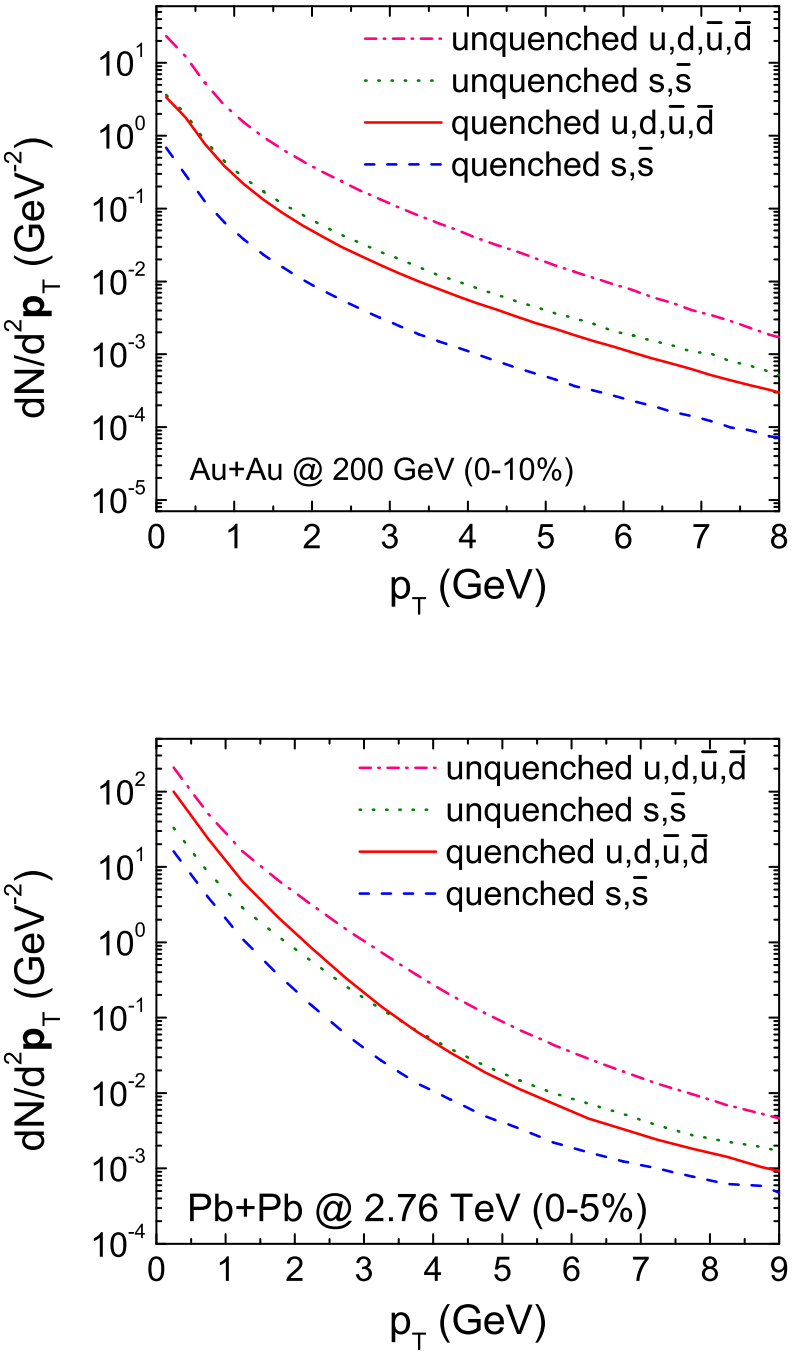

Figure 6.2: Transverse momentum spectra of unquenched (dash-dotted and dotted curves) and quenched (solid and dashed curves) shower partons produced in central (0-10%) Au+Au collisions at $\sqrt{s_{NN}} = 200$ GeV (upper panel) and central Pb+Pb collisions at $\sqrt{s_{NN}} = 2.76$ TeV (lower window).

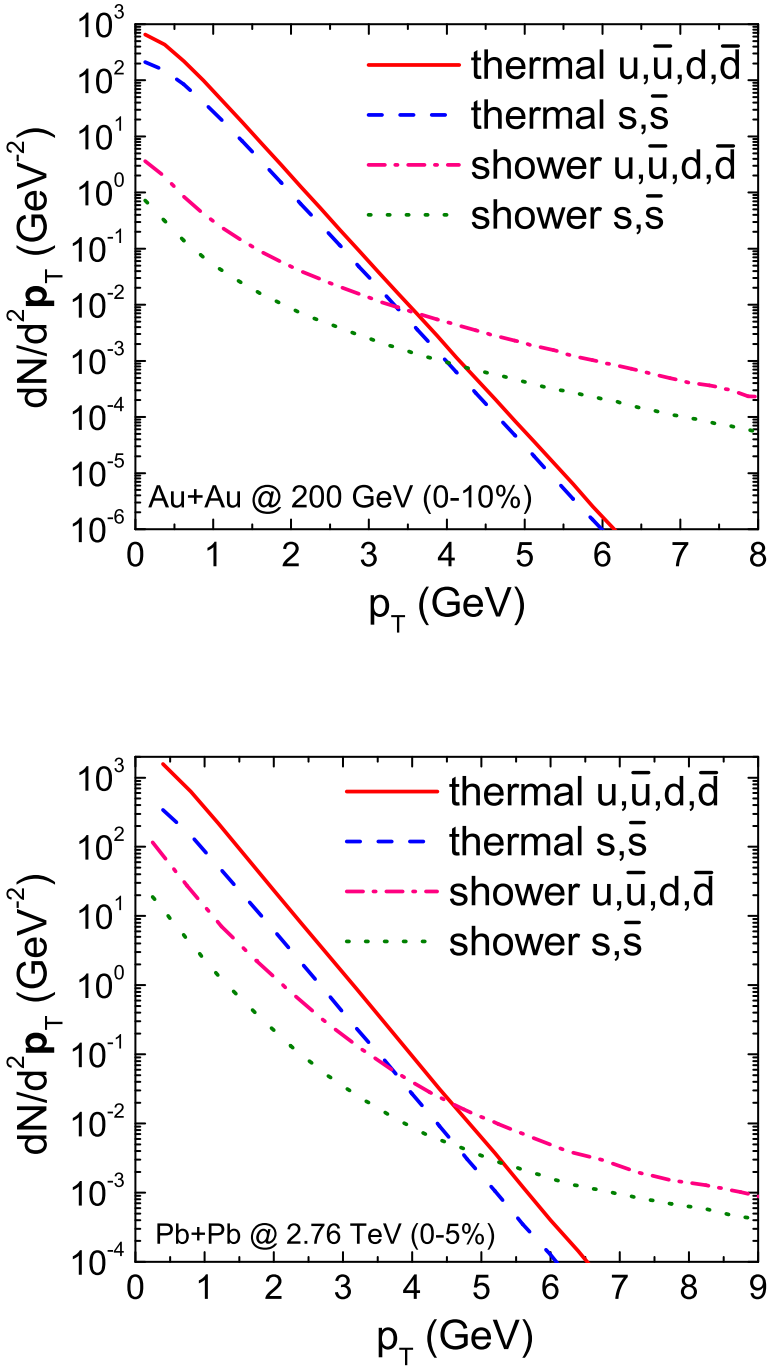

Figure 6.3: Transverse momentum spectra of thermal partons (solid and dashed curves) and quenched shower partons (dash-dotted and dotted curves) produced in Au+Au collisions at $\sqrt{s_{NN}} = 200$ GeV (upper window) and Pb+Pb collisions at $\sqrt{s_{NN}} = 2.76$ TeV (lower window).

In Fig. 6.2, unquenched and quenched shower partons are shown for both cases. We can see that the energy loss at high transverse momenta is larger than that at low transverse momenta because it depends on the energy of shower partons. Figure 6.3 shows the transverse momentum spectra of thermal partons (solid and dashed curves) and the quenched shower partons (dash-dotted and dotted curves) produced in central Au+Au at $\sqrt{s_{NN}} = 200$ GeV (upper window) and in central Pb+Pb collisions at $\sqrt{s_{NN}} = 2.76$ TeV (lower window). These figures show that thermal partons are dominant in the low transverse momentum region (below $p_T \sim 5$ GeV) while shower partons are important in the high momentum region (above $p_T \sim 5$ GeV). For the spatial and time information of shower partons, they are assumed to be distributed uniformly on the transverse plane $z = 0$ of the collision at time $t = 0$. After $t = 0$, shower partons move with their velocities $\mathbf{v} = \mathbf{p}/E$ during their lifetimes, which are assumed to be given by $\tau = \frac{\gamma}{Q}$ in the lab frame, where $\gamma = 1/\sqrt{1 - v^2}$ is the Lorentz dilation factor and Q is the virtuality of the parton. Since the hadronization occurs around τ_c, we propagate all shower partons until their proper times reach τ_c.

6.2 Hadronization of Partons

For the quark recombination, which is based on the sudden approximation, we calculate the overlap of quark and hadron wave functions to find the momentum distributions of mesons and baryons according to Eqs. (4.13) and (4.16). Since the density of thermal partons produced in heavy ion collisions is very high, we do not need to include highly excited states of hadrons, as the overlap of the hadron ground state Wigner function with those of partons is larger than those for excited states. We therefore only consider hadrons obtained from the recombination of thermal partons into the ground state and the decays from the ground state resonances only [11].

The Wigner functions for meson and baryon in their ground states are simply given by Gaussian functions,

$$W_M(y,k) = 8\exp\left(-\frac{y^2}{\sigma_M^2} - k^2\sigma_M^2\right) \tag{6.4}$$

$$W_B(y_1,y_2;k_1,k_2) = 64\exp\left(-\frac{y_1^2}{\sigma_{B1}^2} - \frac{y_2^2}{\sigma_{B2}^2} - k_1^2\sigma_{B1}^2 - k_2^2\sigma_{B2}^2\right). \tag{6.5}$$

For hadron production, we treat three contributions separately: recombination of thermal partons among themselves, of shower and thermal partons, and of shower partons among themselves. We further include the string fragmentation of remnant shower partons. While there are a large number of thermal partons produced in central heavy ion collisions, their number at the intermediate momentum region, in which their recombination with shower partons mostly occurs, is very small, and we thus employ the *test parton method* for the recombination of shower and thermal partons [11]. For the formation of meson and baryon from thermal partons, the coalescence formulas Eqs. (4.13) and (4.16) shown in Section 4 are rewritten as

$$\begin{aligned}\frac{dN_M}{d^3\mathbf{K}_M} &= g_M \int d^3\mathbf{x}_1 d^3\mathbf{k}_1 d^3\mathbf{x}_2 d^3\mathbf{k}_2 P_q(k_{1T}) \frac{dN_q}{d^3\mathbf{x}_1 d^3\mathbf{k}_1} \\ &\times P_{\bar{q}}(k_{2T}) \frac{dN_{\bar{q}}}{d^3\mathbf{x}_2 d^3\mathbf{k}_2} W_M(\mathbf{y},\mathbf{k}) \delta^{(3)}(\mathbf{K}_M - \mathbf{k}_1 - \mathbf{k}_2)\end{aligned} \tag{6.6}$$

$$\begin{aligned}\frac{dN_B}{d^3\mathbf{K}_B} &= g_B \int d^3\mathbf{x}_1 d^3\mathbf{k}_1 d^3\mathbf{x}_2 d^3\mathbf{k}_2 d^3\mathbf{x}_3 d^3\mathbf{k}_3 P_{q_1}(k_{1T}) \frac{dN_q}{d^3\mathbf{x}_1 d^3\mathbf{k}_1} P_{q_2}(k_{2T}) \\ &\times \frac{dN_{q_2}}{d^3\mathbf{x}_2 d^3\mathbf{k}_2} P_{q_3}(k_{3T}) \frac{dN_{q_3}}{d^3\mathbf{x}_3 d^3\mathbf{k}_3} W_B(\mathbf{y}_1,\mathbf{y}_2;\mathbf{k}_1,\mathbf{k}_2) \delta^{(3)}(\mathbf{K}_B - \sum_{i=1}^{3} \mathbf{k}_i)\end{aligned} \tag{6.7}$$

where $P_q(k_T)$ and $P_{\bar{q}}(k_T)$ are the probabilities carried by test thermal quark and thermal antiquark with values proportional to their transverse momentum spectra

at k_T and g_M and g_B denote statistical factors for meson and baryon that include spin and color degeneracies. In our study, we consider g_π=g_K = 1/36, g_ρ = g_{K^*} = 1/12, g_p = 1/108, and g_Δ = 1/54 for the recombination of thermal partons among themselves while using the same values as we used in Section 4 for the recombination of thermal partons with shower ones as well as for that of shower partons among themselves. By using the Monte Carlo method, the numbers of recombined mesons of momentum $\mathbf{K}_M$ and baryons of momentum $\mathbf{K}_B$ are given by

$$N_M(\mathbf{K}_M) = g_M \sum_{i,j} P_q(i) P_{\bar{q}}(j) W_M(x_i, x_j; k_i, k_j) \tag{6.8}$$

$$N_B(\mathbf{K}_B) = g_B \sum_{i \neq j \neq k} P_{q_1}(i) P_{q_2}(j) P_{q_3}(k) W_B(x_i, x_j, x_k; k_i, k_j, k_k), \tag{6.9}$$

$$\tag{6.10}$$

where $\mathbf{K}_M = \mathbf{k}_i + \mathbf{k}_j$ and $\mathbf{K}_B = \mathbf{k}_i + \mathbf{k}_j + \mathbf{k}_k$, shower partons having probabilities of one.

The recombination of shower partons among themselves should mainly contribute to hadron production in the high momentum region. However, there remain shower partons that cannot find partner partons to recombine at high momenta. Those remnant shower partons at high transverse momenta will fragment into hadrons via string fragmentation as in the vacuum (see Section 4). In addition, since the fraction of shower partons that recombine with thermal partons are small ($\sim$ 2%), we do not subtract their number in calculating the recombination of shower partons among themselves. In calculating hadron production from thermal-thermal and thermal-shower recombinations, we include ρ and K^* for meson resonances and Δ for baryon resonances, and all of them finally decay into pions, kaons, and nucleons. Although there could be decays of other unstable hadronic resonances, their contributions are

not significant, so we do not include them in our study. We use the same width parameters in the meson and baryon Wigner functions as used in Section 4.

6.3 Hadron Production via Parton Recombination at RHIC and LHC

We treat separately the three components of quark recombination for hadronization described in the previous section. In order to demonstrate more clearly the effect of medium modification of jet fragmentation, we show the transverse momentum spectra of hadrons with and without contributions from the recombination of shower and thermal partons and compare them with results measured at RHIC and LHC. We first obtain hadron transverse momentum spectra from the recombination of thermal partons among themselves. We then calculate the transverse momentum spectra from recombination of shower partons with thermal partons. The final spectra are obtained by adding the contribution from all components, including those from the shower-shower recombination and the string fragmentation of remnant partons. In Fig. 6.4, we show the pion transverse momentum spectra with and without the contribution of shower-thermal recombination obtained in central Au+Au collisions (0-10 %) at $\sqrt{s_{NN}} = 200$ GeV (upper window) and central Pb+Pb collisions (0-5 %) at $\sqrt{s_{NN}} = 2.76$ TeV (lower window). The dashed-dotted curves indicate that the recombination of shower partons among themselves and the fragmentation of remnant partons are important at high momenta. In the inset of these figures, the ratio of those with and without the shower-thermal recombination is shown. Filled circles in Fig. 6.4 are pion transverse momentum spectra obtained from experiments at RHIC [4] and LHC [5]. Fig. 6.5 and Fig. 6.6 show the same results for kaons and protons. The transverse momentum spectra including contributions from the shower-thermal recombination for pion, kaon, and proton indicated by dashed curves agree well with the experimental results from RHIC [4, 6] and LHC [5]. The ratios given

in the insets of Fig. 6.4, Fig. 6.5, and Fig. 6.6, clearly show the enhancement at intermediate transverse momenta due to the recombination of thermal partons with shower partons. In Table 6.3, we give the positions and heights of the peaks in the ratios of the hadron transverse momentum spectra with and without the contribution from the recombination of shower and therml partons in central Au+Au collisions at $\sqrt{s_{NN}} = 200$ GeV and in central Pb+Pb collisions at $\sqrt{s_{NN}} = 2.76$ TeV. These

Table 6.3: Positions and heights of peaks in the ratios of the hadron transverse momentum spectra with and without contributions of thermal-shower recombination obtained from Au+Au at $\sqrt{s_{NN}} = 200$ GeV and Pb+Pb at $\sqrt{s_{NN}} = 2.76$ TeV.

	RHIC			LHC		
	π^0	K^-	$\bar{p}$	$\pi^+ + \pi^-$	$K^+ + K^-$	$p + \bar{p}$
Positions of Peaks	3.5 GeV	4 GeV	5.5 GeV	5 GeV	5 GeV	6 GeV
Heights of Peaks	2.2	2.0	5.0	2.6	3.1	6.5

results indicate that the peaks at LHC are shifted to higher transverse momenta compared to those at RHIC, and the heights of these peaks at LHC are larger than those at RHIC. This is reasonable because the number of partons produced at LHC are larger than that at RHIC and partons at LHC are also more energetic than those at RHIC.

In Fig. 6.7, we show the ratios of $\bar{p}$ to π^+ at RHIC (upper window) and $p + \bar{p}$ to $\pi^+ + \pi^-$ at LHC (lower window) as functions of transverse momenta. Excluding the contributions from the coalescence of shower partons in jets with the thermal partons in QGP, the ratios are represented by the dashed curve, whose peak has a value of 0.8 at p_T around 2.25 GeV at RHIC and of 0.75 at p_T around 3.0 GeV at LHC. Including the contributions from the coalescence of shower partons with

thermal partons, the ratios are shown by the solid lines that has a peak value of 0.9 at p_T around 2.5 GeV at RHIC and of 0.9 at p_T around 3.5 GeV at LHC. The filled circles represent the results from experimental data at RHIC [44] and LHC [8]. These results indicate that the coalescence of shower partons with thermal partons provides a convincing evidence that medium effects are responsible for the anomalous enhancement in the measured pion to proton ratios in the intermediate momentum region. It results from the fact that the proton spectra are enhanced more than the pion spectra, especially in the intermediate momentum region.

Dividing the hadron transverse momentum spectra obtained with quenched shower partons by those with unquenched shower partons, the nuclear modification factor $R_{\rm AA}$ for hadron spectra can be calculated as follows;

$$R_{\rm AA} = \frac{dN_{\rm quenched}/d^2\mathbf{p}_T}{dN_{\rm unquenched}/d^2\mathbf{p}_T}. \tag{6.11}$$

In Fig. 6.8, we show the R_{AA} of pions at RHIC (upper window) and LHC (lower window). The filled stars indicate the R_{AA} of pions obtained by using Eq. (6.11) while the filled squares are the results from the experimental data measured at RHIC [9] and LHC [5]. It is seen that the $R_{\rm AA}$ of pions obtained from our calculation for RHIC and LHC agrees well with that from the experimental data except in the low transverse momentum region.

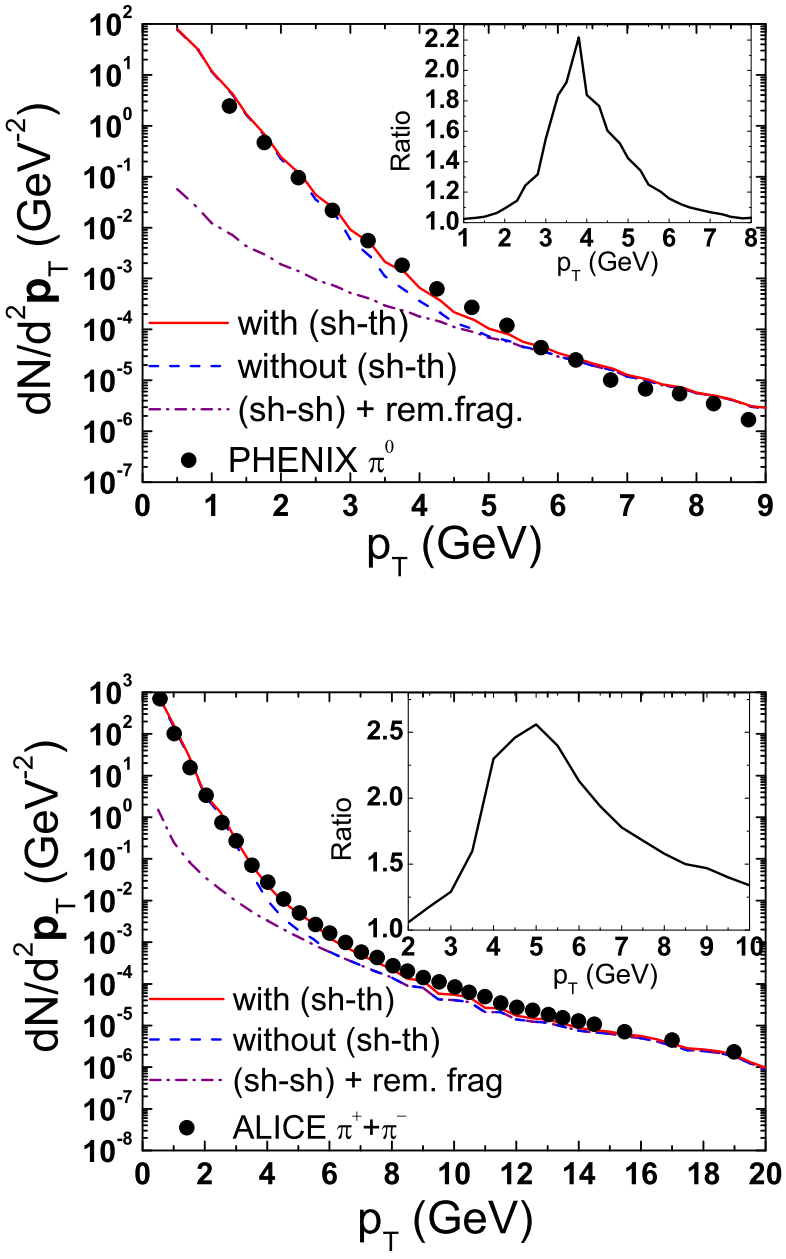

Figure 6.4: Transverse momentum spectra of pions produced from central (0-10% Au+Au collisions (upper window) at $\sqrt{s_{NN}} = 200$ GeV and central (0-5%) Pb+Pb collisions at $\sqrt{s_{NN}} = 2.76$ TeV (lower window) with (solid curves) and without (dashed curves) contributions from coalescence of shower partons with thermal partons in QGP. The dashed-dotted curves show the contributions from the sum of the recombination of shower partons and the fragmentation of remnant partons. Ratio of those two spectra is shown in the inset. Filled circles indicate transverse momentum spectra of π^0 measured at RHIC [4] and $\pi^+ + \pi^-$ measured at LHC [5].

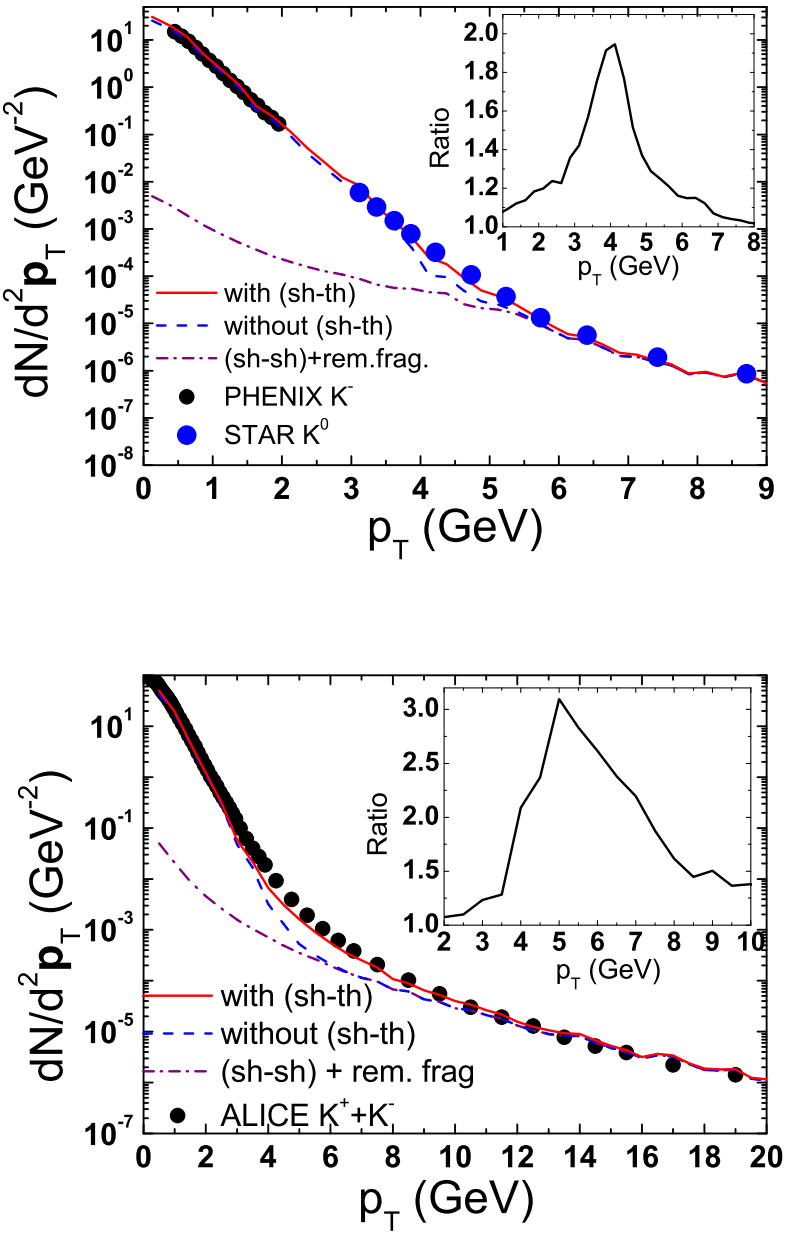

Figure 6.5: Transverse momentum spectra of kaons produced from central (0-10%) Au+Au collisions at $\sqrt{s_{NN}} = 200$ GeV (upper window) and central (0-5%) Pb+Pb collisions at $\sqrt{s_{NN}} = 2.76$ TeV (lower window) with (solid curves) and without (dashed curves) contributions from coalescence of shower partons with thermal partons in QGP. Ratios of the two spectra are shown in the insets. Dash-dotted curves show contributions from sum of the recombination of shower partons and the string fragmentation of remnant partons. Filled circles indicate transverse momentum spectra of kaons measured at RHIC [6, 7] and $K^+ + K^-$ at LHC [5].

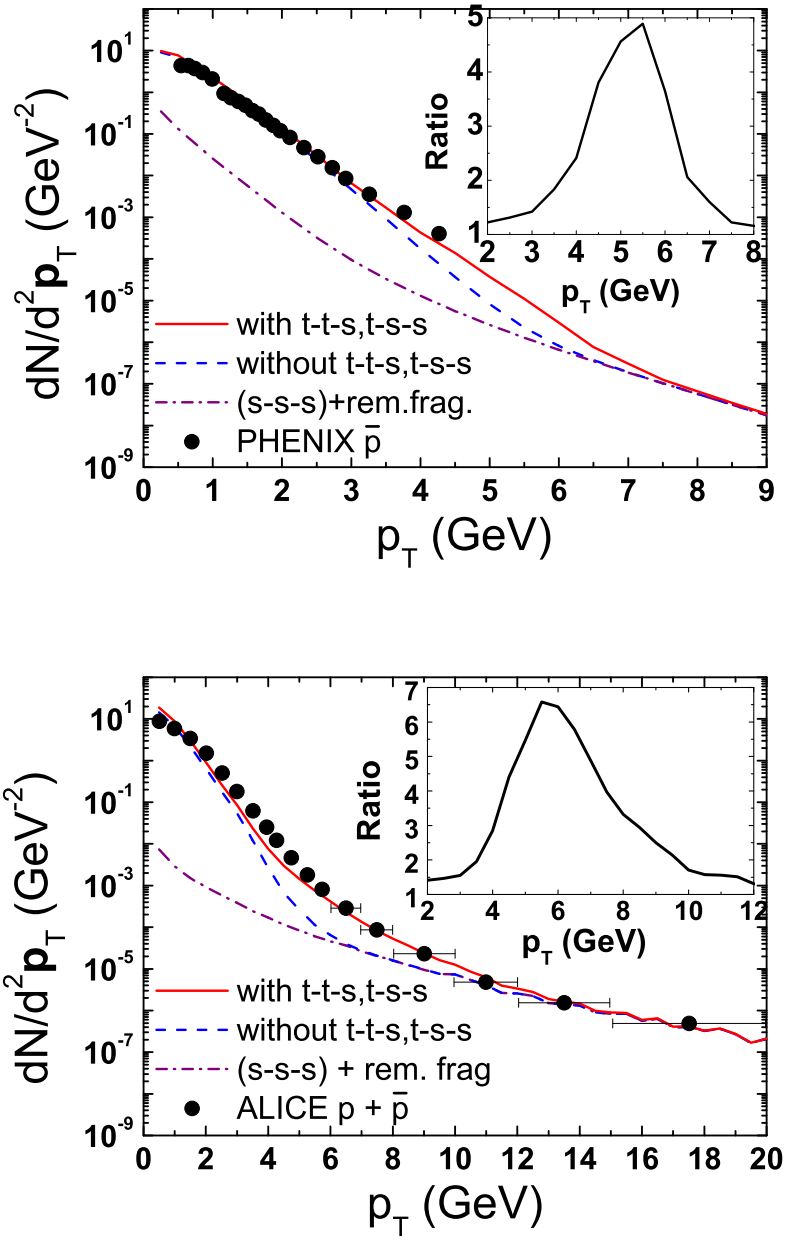

Figure 6.6: Transverse momentum spectra of antiprotons produced from central Au+Au collisions at $\sqrt{s_{NN}} = 200$ GeV (upper window) and central Pb+Pb collisions at $\sqrt{s_{NN}} = 2.76$ TeV (lower window) with (solid curves) and without (dashed curves) contributions from coalescence of shower partons with thermal partons in QGP. Ratio of the two spectra is shown in the inset. Dash-dotted curves show contributions from the sum of the recombination of shower partons and the string fragmentation of remnant partons. Filled circles indicate transverse momentum spectra of $\bar{p}$ measured at RHIC [4] and $p + \bar{p}$ at LHC [5].

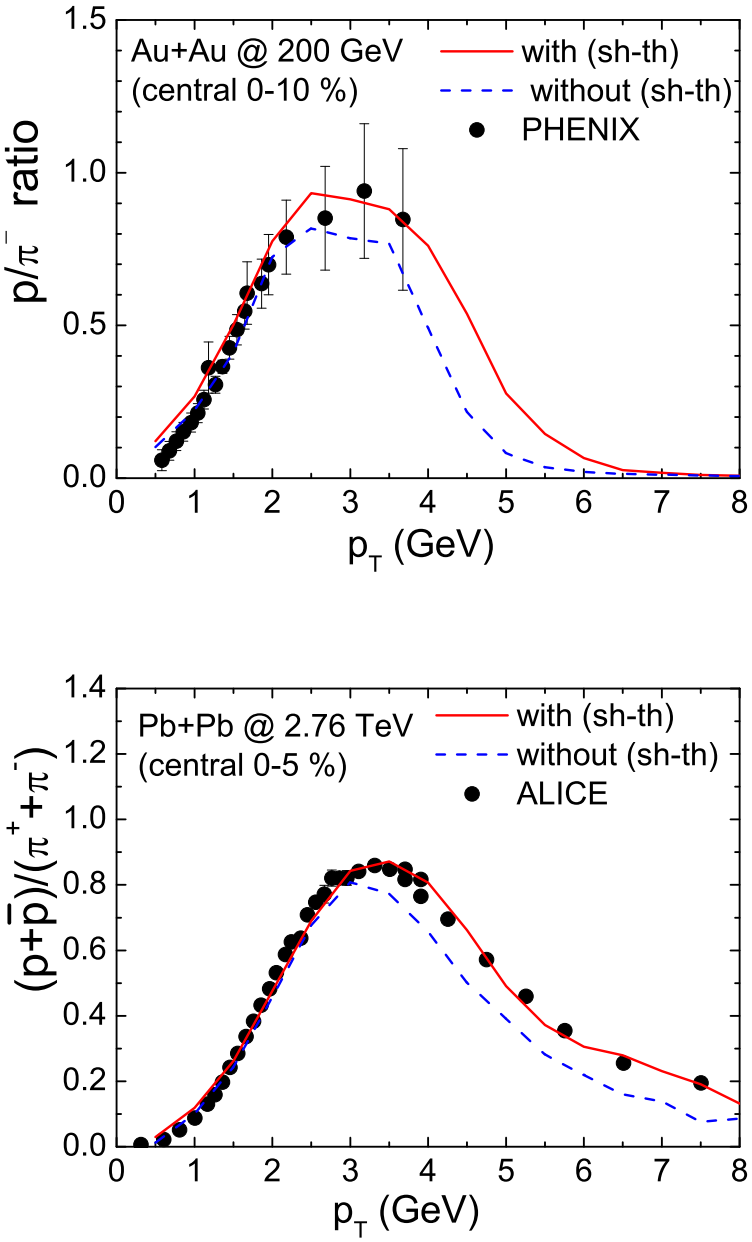

Figure 6.7: The ratios of $\bar{p}$ to π^+ at RHIC (upper window) and of $p+\bar{p}$ to $\pi^+ + \pi^-$ at LHC (lower window). Solid and dashed curves are results with and without contributions from the recombination of shower partons with thermal partons, respectively. Filled circles are experimental data measured at RHIC [4] and LHC [8].

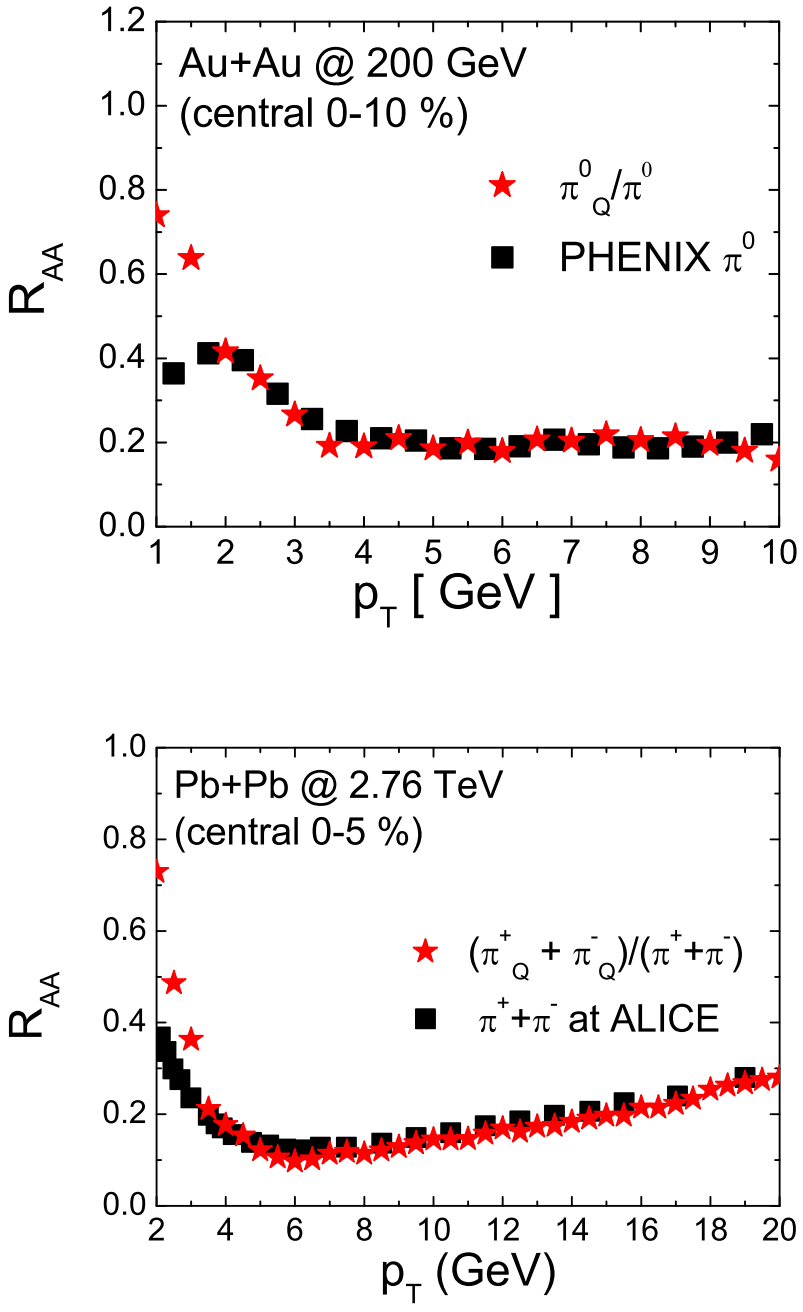

Figure 6.8: Nuclear modification factor R_{AA} of π^0 obtained from our calculation (filled stars) in central Au+Au collisions at $\sqrt{s_{NN}} = 200$ GeV (upper window) and of $\pi^+ + \pi^-$ in central Pb+Pb collisions at $\sqrt{s_{NN}} = 2.76$ TeV (lower window). Filled squares are experimental data measured at RHIC [9] and LHC [5].

7. CONCLUSIONS AND OUTLOOK

The quark recombination model is a useful model for studying the effects of medium on the hadronization of jets into hadrons in the intermediate momentum region. To demonstrate this, we have first reproduced jet fragmentation in vacuum by using a hybrid model that includes the coalescence of shower partons and the string fragmentation of remaining partons. For this study, we have used PYTHIA event generator to obtain parton showers produced from 2-jet events in $e^+ + e^-$ collisions. At the end of perturbative evolution, gluons are decayed non-perturbatively into pairs of quark and antiquark. Since PYTHIA does not give any space-time information for shower partons, they are obtained in the present study by assuming that the average lifetimes of partons are determined by the inverses of their virtualities. Using the hadron Wigner functions based on the harmonic oscillator wave functions, we have recombined partons into hadrons in an event-by-event basis. Since the number of shower partons in each event is small and their distribution in phase space is dilute, we have included highly excited hadrons in the recombination calculations to enhance their recombination probabilities. Also, we have introduced Gaussian wave packets for shower partons to take into account their space-momentum uncertainties. This then leads to the wave packet weighted or Gaussian smeared hadron Wigner functions. We have further derived general formula for evaluating these Gaussian smeared Wigner functions and included the decays of hadron resonances with high excitation energies. For partons that are not converted into hadrons after recombination, we allow them to form strings to fragment into hadrons. After adding contributions from the recombination of shower partons and the string fragmentation of remnant partons, we could reproduce well the momentum spectra of pion,

kaon, nucleon, and Λ given by the string fragmentation in PYTHIA.

The above study is then extended to include the medium modification of jet fragmentation in relativistic heavy ion collisions via recombination of shower partons with thermal partons in the produced QGP from central Au+Au collisions at $\sqrt{s_{NN}} = 200$ GeV available at RHIC and from central Pb+Pb collisions at $\sqrt{s_{NN}} = 2.76$ TeV available at LHC. The latter is obtained from a blast wave model using the test particle method. In this method, thermal partons are not physical particles but test particles with their probabilities proportional to their transverse momentum spectra. For the transverse momentum spectra of jets produced in central heavy ion collisions, they are obtained from the jets in a $p + p$ collision using the Monte Carlo event generator PYTHIA multiplied by the number of binary collisions. Fitting the obtained transverse momentum spectra of jets with a power law, we further generate jets and branch them into parton showers by using the subroutine PYSHOW in PYTHIA. In each branching, we have included its energy loss using one of the opacity expansion approaches. We have classified hadron production in heavy ion collisions into three components: recombination of thermal partons among themselves, that of thermal partons with shower partons, and that of shower partons among themselves plus the string fragmentation of remnant shower partons. For the thermal-thermal recombination, which is important in the low momentum region, it is carried out by simply adding the hadron Wigner functions from recombining the test partons. For the shower-thermal recombination, we also use the test parton method. The recombination of shower partons among themselves are treated exactly the same way as their recombination in the vacuum with the remanent partons converted to hadrons via string fragmentation. We have added the contributions from all three contributions and compared the resulting transverse momentum spectra of hadrons with and without the shower-thermal recombination. Our results show that the trans-

verse momentum spectra of hadrons are enhanced in the intermediate momentum region. Also, we have shown that the ratio of the proton number to that of pions is increased in the intermediate momentum region. We have compared our results with those from experimental measurements at RHIC and LHC found they agree well with each other.

To conclude, our new recombination model can describe well the medium modification of jet fragmentation as well as the anomalies observed in the ratio of baryons to mesons seen in the experimental data. For a more realistic study, we need to use hydrodynamical approach for treating thermal partons in a QGP rather than the blast wave model. In this case, we need to treat the energy loss of shower partons on a cell-by-cell basis. Also, for the jet fragmentation in vacuum, we have not used physical resonances but have just let the excited hadron states to decay into 2-body, 3-body, and 4-body final states. Ultimately, we need to include all baryons and mesons given in the list of known hadron resonances [10] and decay them according to their empirical decay modes. These studies will be left for the future.

REFERENCES

[1] W. J. S. R. K. Ellis and B. R. Webber, *QCD and Collider Physics* (Cambridge University Press, Cambridge, United Kingdom, 2003).

[2] B. Webber, Nucl. Phys. B **238**, 492 (1984).

[3] K. C. Han, R. J. Fries, and C. M. Ko, Phys. Rev. **C93**, 045207 (2016), 1601.00708.

[4] PHENIX, S. S. Adler *et al.*, Phys. Rev. C **69**, 034909 (2004), nucl-ex/0307022.

[5] ALICE Collaboration, B. Abelev *et al.*, Phys. Rev. Lett. **109**, 252301 (2012), 1208.1974.

[6] PHENIX, K. Adcox *et al.*, Phys. Rev. Lett. **88**, 022301 (2002), nucl-ex/0109003.

[7] STAR, G. Agakishiev *et al.*, Phys. Rev. Lett. **108**, 072302 (2012), 1110.0579.

[8] ALICE, B. B. Abelev *et al.*, Phys. Lett. B **736**, 196 (2014), 1401.1250.

[9] PHENIX, M. Naglis, Nucl. Phys. A **830**, 757C (2009), 0907.4461.

[10] Particle Data Group, J. Beringer *et al.*, Phys. Rev. D **86**, 010001 (2012).

[11] V. Greco, C. Ko, and P. Levai, Phys. Rev. C **68**, 034904 (2003), nucl-th/0305024.

[12] J. C. Collins and D. E. Soper, Nucl. Phys. B **194**, 445 (1982).

[13] R. Field and R. Feynman, Nucl. Phys. B **136**, 1 (1978).

[14] V. Greco, C. Ko, and P. Levai, Phys. Rev. Lett. **90**, 202302 (2003), nucl-th/0301093.

[15] R. Fries, B. Muller, C. Nonaka, and S. Bass, Phys. Rev. C **68**, 044902 (2003), nucl-th/0306027.

[16] R. C. Hwa and C. Yang, Phys. Rev. C **70**, 024904 (2004), hep-ph/0312271.

[17] X.-N. Wang and M. Gyulassy, Phys. Rev. Lett. **68**, 1480 (1992).

[18] A. Majumder and M. Van Leeuwen, Prog. Part. Nucl. Phys. A **66**, 41 (2011), 1002.2206.

[19] H. Zhang, J. F. Owens, E. Wang, and X.-N. Wang, Phys. Rev. Lett. **98**, 212301 (2007), nucl-th/0701045.

[20] H. Zhang, J. F. Owens, E. Wang, and X.-N. Wang, Phys. Rev. Lett. **103**, 032302 (2009), 0902.4000.

[21] H. Zhang, T. Song, and C. M. Ko, Phys. Rev. C **87**, 054902 (2013), 1208.2980.

[22] T. Sjostrand, S. Mrenna, and P. Z. Skands, JHEP **0605**, 026 (2006), hep-ph/0603175.

[23] X. Artru and G. Mennessier, Nucl. Phys. B **70**, 93 (1974).

[24] B. Andersson, G. Gustafson, G. Ingelman, and T. Sjostrand, Phys. Rept. **97**, 31 (1983).

[25] M. Bowler, Z. Phys. C **11**, 169 (1981).

[26] B. Andersson, G. Gustafson, and B. Soderberg, Nucl. Phys. B **264**, 29 (1986).

[27] T. Sjostrand, Nucl. Phys. B **248**, 469 (1984).

[28] J. S. Schwinger, Phys. Rev. **82**, 664 (1951).

[29] D. Amati and G. Veneziano, Phys. Lett. B **83**, 87 (1979).

[30] STAR Collaboration, J. Adams *et al.*, Nucl. Phys. A **757**, 102 (2005), nucl-ex/0501009.

[31] PHENIX Collaboration, K. Adcox *et al.*, Nucl. Phys. A **757**, 184 (2005), nucl-ex/0410003.

[32] S. Voloshin, Nucl. Phys. A **715**, 379 (2003), nucl-ex/0210014.

[33] D. Molnar and S. A. Voloshin, Phys. Rev. Lett. **91**, 092301 (2003), nucl-th/0302014.

[34] R. C. Hwa and C. Yang, Phys. Rev. C **67**, 064902 (2003), nucl-th/0302006.

[35] R. Fries, B. Muller, C. Nonaka, and S. Bass, Phys. Rev. Lett. **90**, 202303 (2003), nucl-th/0301087.

[36] R. J. Fries, V. Greco, and P. Sorensen, Ann. Rev. Nucl. Part. Sci. **58**, 177 (2008), 0807.4939.

[37] R. C. Hwa and C. Yang, Phys. Rev. C **70**, 024905 (2004), nucl-th/0401001.

[38] Y. L. Dokshitzer, Sov. Phys. JETP **46**, 641 (1977).

[39] G. Altarelli and G. Parisi, Nucl. Phys. B **126**, 298 (1977).

[40] V. Gribov and L. Lipatov, Sov. J. Nucl. Phys. **15**, 438 (1972).

[41] V. Sudakov, Sov. Phys. JETP **3**, 65 (1956).

[42] K. C. Zapp, *A Monte Carlo model for jet evolution with energy loss*, PhD thesis, Heidelberg U., 2008.

[43] G. Corcella *et al.*, (2002), hep-ph/0210213.

[44] PHENIX, S. S. Adler *et al.*, Phys. Rev. Lett. **91**, 072301 (2003), nucl-ex/0304022.

[45] K. Das and R. C. Hwa, Phys. Lett. B **68**, 459 (1977).

[46] B. Muller, R. J. Fries, and S. A. Bass, Phys. Lett. B **618**, 77 (2005), nucl-th/0503003.

[47] K. C. Han, R. J. Fries, and C. M. Ko, J. Phys. Conf. Ser. **420**, 012044 (2013), 1209.1141.

[48] E. Merzbacher, *Quantum Mechanics*, 3rd ed. (John Wiley & Sons, Inc., New Jersey, the United States, 1997).

[49] D. Amati, R. Petronzio, and G. Veneziano, Nucl. Phys. B **146**, 29 (1978).

[50] J. F. Amundson, O. J. P. Eboli, E. M. Gregores, and F. Halzen, Phys. Lett. B **390**, 323 (1997), hep-ph/9605295.

[51] F. Halzen, Phys. Lett. B **69**, 105 (1977).

[52] H. Fritzsch, Phys. Lett. B **67**, 217 (1977).

[53] L.-W. Chen, C. Ko, and B.-A. Li, Nucl. Phys. A **729**, 809 (2003), nucl-th/0306032.

[54] L.-W. Chen and C. M. Ko, Phys. Rev. C **73**, 044903 (2006), nucl-th/0602025.

[55] Y. Oh, C. M. Ko, S. H. Lee, and S. Yasui, Phys. Rev. C **79**, 044905 (2009), 0901.1382.

[56] C. M. Ko, T. Song, F. Li, V. Greco, and S. Plumari, Nucl. Phys. A **928**, 234 (2014), 1211.5511.

[57] R. H. Milburn, Rev. Mod. Phys. **27**, 1 (1955).

[58] J. Bjorken, Fermilab-Pub-82/59-THY (1982).

[59] M. H. Thoma, Phys. Lett. B **273**, 128 (1991).

[60] M. G. Mustafa and M. H. Thoma, Acta Phys. Hung. A **22**, 93 (2005), hep-ph/0311168.

[61] M. G. Mustafa, Phys. Rev. C **72**, 014905 (2005), hep-ph/0412402.

[62] M. Gyulassy and M. Plumer, Phys. Lett. B **243**, 432 (1990).

[63] M. Gyulassy and X.-n. Wang, Nucl. Phys. B **420**, 583 (1994), nucl-th/9306003.

[64] R. Baier, D. Schiff, and B. G. Zakharov, Ann. Rev. Nucl. Part. Sci. **50**, 37 (2000), hep-ph/0002198.

[65] B. G. Zakharov, JETP Lett. **70**, 176 (1999), hep-ph/9906536.

[66] U. A. Wiedemann, Nucl. Phys. B **588**, 303 (2000), hep-ph/0005129.

[67] C. A. Salgado and U. A. Wiedemann, Phys. Rev. Lett. **89**, 092303 (2002), hep-ph/0204221.

[68] C. A. Salgado and U. A. Wiedemann, Phys. Rev. D **68**, 014008 (2003), hep-ph/0302184.

[69] M. Gyulassy, P. Levai, and I. Vitev, Nucl. Phys. B **571**, 197 (2000), hep-ph/9907461.

[70] M. Gyulassy, P. Levai, and I. Vitev, Phys. Rev. Lett. **85**, 5535 (2000), nucl-th/0005032.

[71] M. Gyulassy, P. Levai, and I. Vitev, Phys. Lett. B **538**, 282 (2002), nucl-th/0112071.

[72] M. Gyulassy, P. Levai, and I. Vitev, Nucl. Phys. B **594**, 371 (2001), nucl-th/0006010.

[73] X.-f. Guo and X.-N. Wang, Phys. Rev. Lett. **85**, 3591 (2000), hep-ph/0005044.

[74] X.-N. Wang and X.-f. Guo, Nucl. Phys. A **696**, 788 (2001), hep-ph/0102230.

[75] A. Majumder, C. Nonaka, and S. A. Bass, Phys. Rev. C **76**, 041902 (2007), nucl-th/0703019.

[76] P. B. Arnold, G. D. Moore, and L. G. Yaffe, JHEP **06**, 030 (2002), hep-ph/0204343.

[77] P. B. Arnold, G. D. Moore, and L. G. Yaffe, JHEP **01**, 030 (2003), hep-ph/0209353.

[78] S. Jeon and G. D. Moore, Phys. Rev. C **71**, 034901 (2005), hep-ph/0309332.

[79] S. Turbide, C. Gale, S. Jeon, and G. D. Moore, Phys. Rev. C **72**, 014906 (2005), hep-ph/0502248.

[80] G.-Y. Qin *et al.*, Phys. Rev. C **76**, 064907 (2007), 0705.2575.

[81] M. Gyulassy, I. Vitev, and X. N. Wang, Phys. Rev. Lett. **86**, 2537 (2001), nucl-th/0012092.

[82] E. Wang and X.-N. Wang, Phys. Rev. Lett. **87**, 142301 (2001), nucl-th/0106043.

[83] X.-N. Wang, Phys. Rev. C **70**, 031901 (2004), nucl-th/0405029.

[84] X.-N. Wang, Phys. Lett. B **595**, 165 (2004), nucl-th/0305010.

[85] X.-N. Wang, Phys. Rev. C **61**, 064910 (2000), nucl-th/9812021.

[86] A. D. Martin, R. G. Roberts, W. J. Stirling, and R. S. Thorne, Eur. Phys. J. C **4**, 463 (1998), hep-ph/9803445.

[87] S.-y. Li and X.-N. Wang, Phys. Lett. B **527**, 85 (2002), nucl-th/0110075.

[88] K. J. Eskola, V. J. Kolhinen, and C. A. Salgado, Eur. Phys. J. C **9**, 61 (1999), hep-ph/9807297.

[89] E. Wang and X.-N. Wang, Phys. Rev. Lett. **89**, 162301 (2002), hep-ph/0202105.

[90] J. Binnewies, B. A. Kniehl, and G. Kramer, Z. Phys. C **65**, 471 (1995), hep-ph/9407347.

[91] STAR, C. Adler *et al.*, Phys. Rev. Lett. **89**, 202301 (2002), nucl-ex/0206011.

[92] STAR, J. Adams *et al.*, Phys. Rev. Lett. **91**, 172302 (2003), nucl-ex/0305015.

[93] STAR, C. Adler *et al.*, Phys. Rev. Lett. **90**, 082302 (2003), nucl-ex/0210033.

[94] STAR, J. Adams *et al.*, Phys. Rev. Lett. **95**, 152301 (2005), nucl-ex/0501016.

[95] J. Bjorken and E. A. Paschos, Phys. Rev. **185**, 1975 (1969).

[96] Particle Data Group, C. Amsler *et al.*, Phys. Lett. B **667**, 1 (2008).

[97] H. Groenewold, Physica **12**, 405 (1946).

[98] J. Mathews and R. L. Walker, *Mathematical Methods of Physics*, 2nd ed. (Addison-Wesley Publishing Company, Inc., Boston, the United States, 1970).

[99] J. J. Sakurai, *Modern Quantum Mechanics*, Revised ed. (Addison-Wesley Publishing Company, Inc., Boston, the United States, 1985).

APPENDIX A

THE DECAY RATE OF A GLUON INTO A PAIR OF QUARK AND ANTIQUARK

When we recombine shower partons into hadrons, the shower gluons generated from PYTHIA are forced to decay into pairs of quark and antiquark. We need to calculate the decay rate of this process, which is illustrated by the Feynman diagram in Fig. A.1. This can be obtained from the differential decay width [96]

$$d\Gamma = \frac{1}{32\pi^2}\overline{|\mathcal{M}|^2}\frac{|\mathbf{p}_1|^2}{M^2}d\Omega, \tag{A.1}$$

where $\mathcal{M}$, $\mathbf{p}_1$, and M are the invariant amplitude of the decay process, momentum of a produced parton, and the mass of the initial parton, respectively; and $d\Omega \equiv d\phi_1 d(\cos\theta_1)$ is the differential solid angle. In the rest frame of the initial parton,

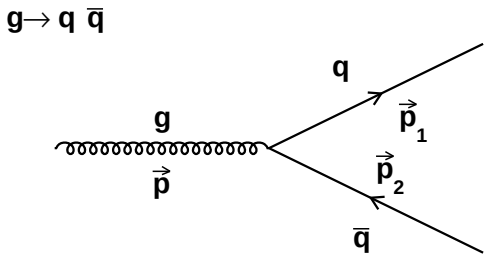

Figure A.1: Feynman diagram for the decay of gluon $g \to q\bar{q}$.

we have

$$|\mathbf{p}_1| = |\mathbf{p}_2| = \frac{\sqrt{[M-(m_1+m_2)^2][M^2-(m_1-m_2)^2]}}{2M},$$
$$E_1 = \frac{M^2-m_2^2+m_1^2}{2M}, \quad E_2 = \frac{M^2-m_1^2+m_2^2}{2M} \tag{A.2}$$

The invariant amplitude is given by

$$\mathcal{M}_{ij} = \bar{u}_i(p_1)(-ig_s\gamma^\mu T^a_{ij})\epsilon_\mu(p)v_j(p_2), \ (i,j=1,2,3, \quad a=1,2,\ldots,8), \tag{A.3}$$

where g_s is a coupling constant, T^a_{ij} are the Gell-Mann matrices, a denotes the gluon color index, $\epsilon^\mu(p)$ is the polarization vector of the initial gluon, and $\bar{u}(p_1)$ and $v(p_2)$ are the Dirac spinors of produced quark and antiquark. The square of the invariant amplitude is then

$$|\mathcal{M}|^2 = \mathcal{M}^\dagger\mathcal{M} = v^\dagger_{j'}(p_2)\epsilon^*_\nu(p)(ig_s\gamma^{\nu^\dagger}(T^a_{i'j'})^\dagger)(\bar{u}_{i'}(p_1))^\dagger\bar{u}_i(p_1)(-ig_s\gamma^\nu T^a_{ij})\epsilon_\mu(p)v_j(p_2). \tag{A.4}$$

Using

$$\sum_s u^s(p_1)\bar{u}^s(p_1) = \not{p}_1 + m_1, \quad \sum_s v^s(p_2)\bar{v}^s(p_2) = \not{p}_2 - m_2$$
$$\sum_\lambda \epsilon^{(\lambda)*}_\mu(p)\epsilon^{(\lambda)}_\nu = -g_{\mu\nu} + \frac{p_\mu p_\nu}{M^2}, \quad \mathrm{Tr}[T^aT^a] = \frac{N_c^2-1}{2}, \tag{A.5}$$

Eq. (A.4) can be rewritten as

$$\mathcal{M}^2 = 16g_s^2\left[2(p_1\cdot p_2) + 4m_1m_2 + \frac{2(p_1\cdot p)(p_2\cdot p) - p^2(p_1\cdot p_2)}{M^2} - \frac{m_1m_2p^2}{M^2}\right]. \tag{A.6}$$

In the rest frame of the initial parton, we have

$$
\begin{aligned}
& p \cdot p_1 = ME_1, \ p \cdot p_2 = ME_2 \\
& p_1 \cdot p_2 = \frac{(p_1+p_2)^2 - p_1^2 - p_2^2}{2} = \frac{M - m_1^2 - m_2^2}{2}.
\end{aligned} \tag{A.7}
$$

Using Eqs. (A.2) and (A.7), the decay width for the process $g \to q\bar{q}$ is then

$$
\begin{aligned}
\Gamma_{g\to q\bar{q}} &= \frac{1}{32\pi^2}\overline{|\mathcal{M}|^2}\frac{|\mathbf{p}_1|}{M^2}\int d\Omega \\
&= \frac{1}{8\times 2}\frac{8g_s^2}{M^2}[2M^4 - (m_1^2 - m_2^2)^2 \\
&- M^2(m_1^2 - 6m_1m_2 + m_2^2)]\frac{1}{32\pi^2}\frac{|\mathbf{p}_1|}{M^2}4\pi \\
&= \frac{g_s^2}{32\pi M^5}\sqrt{[M^2-(m_1+m_2)^2][M^2-(m_1-m_2)^2]} \\
&\times \ [2M^4 - (m_1^2 - m_2^2)^2 - M^2(m_1^2 - 6m_1m_2 + m_2^2)]
\end{aligned} \tag{A.8}
$$

The decay rate of a gluon into a pair of quark and antiquark depends on the masses of the quark and antiquark. The ratio of the decay rate for a gluon into a light quark and antiquark pair and that into a strange quark and antiquark pair can thus be written as

$$
\frac{\Gamma(g^* \to u\bar{u}, d\bar{d})}{\Gamma(g^* \to s\bar{s})} = \frac{2(M^2+2m_{u,d}^2)}{M^2+2m_s^2}\sqrt{\frac{M^2-4m_{u,d}^2}{M^2-4m_s^2}}, \tag{A.9}
$$

where $m_{u,d}$ and m_s are the constituent masses of the light and strange quarks, respectively.

APPENDIX B

OVERLAP INTEGRAL OF QUARK AND HADRON GAUSSIAN WIGNER FUNCTIONS

In this appendix, we discuss in details the calculation of the overlap integral of hadron Wigner functions with the quark Wigner functions, specifically for the case that the hadron Winger functions are obtained from the harmonic oscillator wave functions and the quark Wigner functions are obtained from Gaussian wave packets. In this case, we call the overlap integral as the Gaussian smeared Wigner functions of hadrons. Let us start by noting that both the Gaussian wave packets and the harmonic oscillator problem factorize into the three spatial directions. We can thus solve the corresponding one dimensional problem and then readily find the solution in three dimensions.

We start with the well known harmonic oscillator basis in one dimension [48],

$$\phi_n(x) = \left(\frac{m\omega}{\pi\hbar}\right)^{1/4} \frac{1}{\sqrt{2^n n!}} H_n(\xi) e^{-\xi^2/2}, \tag{B.1}$$

where $\xi = \sqrt{\frac{m\omega}{\hbar}}x$, $H_n(\xi)$ are Hermite polynomials and ω is the oscillator frequency. The Wigner transformation of the harmonic oscillator wave functions, defined by

$$W_n(x,k) = \int_{-\infty}^{\infty} d\eta \; e^{ik\eta} \phi_n\left(x + \frac{\eta}{2}\right) \phi_n\left(x + \frac{\eta}{2}\right), \tag{B.2}$$

leads to [97]

$$W_n(u) = 2(-1)^n L_n(u) e^{-u/2}, \tag{B.3}$$

where $u = 2\left(\frac{x^2}{\sigma^2} + \sigma^2 k^2\right)$ with the width $\sigma = \left(\frac{\hbar}{m\omega}\right)^{1/2}$, and the L_n are Laguerre polynomials.

We would like to calculate the overlap integral

$$\overline{W}_n(x,k) \;=\; \int \frac{dx_1' dk_1' dx_2' dk_2'}{(2\pi)^2} W(x_1', k_1') W(x_2', k_2') W_n(x,k), \tag{B.4}$$

of the Wigner function $W_n(x,k)$ with the Wigner functions of Gaussian wave packets

$$W(x_i', k_i') = 2e^{-(x_i'-x_i)^2/\delta^2} e^{-\delta^2(k_i'-k_i)^2},\ i = 1,2, \tag{B.5}$$

that has width δ around centroids x_i and k_i in space and momentum. Here $x = x_1 - x_2$ and $k = (k_1 - k_2)/2$, and the result will only depend on the relative position of centroids $r = x_1 - x_2$ and $p = (k_1 - k_2)/2$.

Using the generating function for Laguerre polynomials [98],

$$\frac{1}{1-t} e^{-\frac{tx}{1-t}} = \sum_{n=0}^{\infty} t^n L_n(x), \tag{B.6}$$

it is straightforward to see that Eq. (B.3) leads to the generating function for the oscillator Wigner functions

$$\frac{2}{1+t} \exp\left(-\frac{1-t}{2(1+t)} u\right) = \sum_{n=0}^{\infty} t^n W_n(u). \tag{B.7}$$

We not that it can be straightforward to show that the sum of $W_n(u)$ is normalized to one, i.e. $\sum_{n=0}^{\infty} W_n(u) = 1$. Carrying out the integrals from Eq. (B.4) on both sides of above equation, we obtain the following generating function for the Gaussian

smeared Wigner function $\overline{W}_n$

$$\frac{2}{(1+t)(1+a\alpha)^{1/2}(1+a\alpha^{-1})^{1/2}}\exp\left(-\frac{ax^2}{(1+a\alpha)\sigma^2}-\frac{ak^2\sigma^2}{1+a\alpha^{-1}}\right)=\sum_{n=0}^{\infty}t^n\overline{W}_n(x,k), \tag{B.8}$$

where $a=\frac{1-t}{1+t}$ and $\alpha=2\delta^2/\sigma^2$. By Taylor expanding the left hand side in t and comparing coefficients of the same powers in t on both sides, we obtain the following recurrence relation for the $\overline{W}_n$:

$$\overline{W}_{n+5}=-\frac{1}{\Lambda_5}(\Lambda_4\overline{W}_{n+4}+\Lambda_3\overline{W}_{n+3}+\Lambda_2\overline{W}_{n+2}+\Lambda_1\overline{W}_{n+1}+\Lambda_0\overline{W}_n), \tag{B.9}$$

where Λ_i $(i=0,1,\ldots,5)$ are given by

$$\begin{aligned}
\Lambda_0 &= -[(1+\alpha)^2+n](1-\alpha)^2,\\
\Lambda_1 &= [\alpha(1-\alpha)+2(x/\sigma)^2+2\alpha^2(k\sigma)^2+n+1](1-\alpha)^2x\\
\Lambda_2 &= [(1-\alpha)(\alpha^2+4\alpha+1)-2(x/\sigma)^2(3\alpha+1)-2\alpha(k\sigma)^2(-\alpha^2+3\alpha+2)\\
&\quad -2(n+2)(1+\alpha)^2(1-\alpha)](1-\alpha),\\
\Lambda_3 &= [\alpha(1-\alpha)^2+2(x/\sigma)^2(3\alpha^2-2\alpha-1)+2\alpha(k\sigma)^2(\alpha^3-3\alpha^2+9\alpha-7)\\
&\quad -2(n+3)(1+\alpha)^2(1-\alpha)^2],\\
\Lambda_4 &= [2(x/\sigma)^2+2\alpha^2(k\sigma)^2-(n+4)(1-\alpha)^2](1+\alpha)^2,\\
\Lambda_5 &= -(n+5)(1+\alpha)^2.
\end{aligned} \tag{B.10}$$

Taking $\alpha=2\delta^2/\sigma^2=1$ for simplicity reduces Eq.(B.9) to

$$\overline{W}_{n+1}=\frac{v}{n+1}\overline{W}_n, \tag{B.11}$$

with

$$\overline{W}_0 = \exp(-v) \quad \text{and} \quad v = \frac{1}{2}\left(\frac{x^2}{\sigma^2} + k^2\sigma^2\right) \tag{B.12}$$

or equivalently

$$\overline{W}_n = \frac{v^n}{n!}e^{-v}. \tag{B.13}$$

The Gaussian smeared $\overline{W}_n$ has the form of a Poisson distribution with the normalization

$$\sum_{n=0}^{\infty} \frac{v^n}{n!}e^{-v} = 1, \tag{B.14}$$

which implies that the coalescing quark and antiquark pair is a coherent state of all formed mesons like the displaced harmonic oscillator ground state [99].

In three dimensions, the Gaussian smeared Wigner function is thus given by

$$\begin{aligned}
\overline{W}_n(\mathbf{x},\mathbf{k}) &= \sum_{n_x+n_y+n_z=n} \overline{W}_{n_x}(x,k_x)\overline{W}_{n_y}(y,k_y)\overline{W}_{n_z}(z,k_z) \\
&= \sum_{n_x+n_y+n_z=n} \frac{v_x^{n_x}}{n_x!}e^{-v_x} \cdot \frac{v_y^{n_x}}{n_y!}e^{-v_y} \cdot \frac{v_z^{n_z}}{n_z!}e^{-v_z} \\
&= \frac{1}{n!}e^{-v} \sum_{n_x+n_y+n_z=n} \frac{n!}{n_x!n_y!n_z!}v_x^{n_x}v_y^{n_y}v_z^{n_z} \\
&= \frac{v^n}{n!}e^{-v},
\end{aligned} \tag{B.15}$$

with

$$v = v_x + v_y + v_z = \frac{1}{2}\left(\frac{\mathbf{x}^2}{\sigma^2} + \mathbf{k}^2\sigma^2\right). \tag{B.16}$$

The fourth equality in Eq.(B.15) follows from using the trinomial expansion formula

$$\sum_{n_x+n_y+n_z=n} = \frac{n!}{n_x!n_y!n_z!} v_x^{n_x} v_y^{n_y} v_z^{n_z} = (v_x + v_y + v_z)^n = v^n. \tag{B.17}$$

APPENDIX C

TWO-BODY AND MANY-BODY DECAYS

C.1 Two-Body Decays

In order to study multi-body decays of a particle, we first need to understand the simplest case, i.e. the two-body decay. Let us consider the two-body decay of a particle with a given mass M and known three-momentum in the lab frame to two particles of masses m_1 and m_2. In the rest frame of the initial particle (Fig. C.1), the four-momentum of the initial particle can be written as $P^\mu = (M, \mathbf{0})$ ($\mu = 0, 1, 2, 3$). After the decay, the energy-momentum conservation gives the energies and momenta of the produced particles as

$$M = E_1 + E_2, \quad \mathbf{p}_1 + \mathbf{p}_2 = \mathbf{0} \tag{C.1}$$

$$E_1 = \sqrt{\mathbf{p}_1^2 + m_1^2}, \quad E_2 = \sqrt{\mathbf{p}_2^2 + m_2^2} \tag{C.2}$$

where $(E_1, \mathbf{p}_1)$ and $(E_2, \mathbf{p}_2)$ are energies and momenta of the produced two particles, respectively. The magnitude of the momenta of produced particles in the rest frame of the initial particle can then be obtained as

$$|\mathbf{p}_1| = |\mathbf{p}_2| = \frac{[M^2 - (m_1 + m_2)^2)(M^2 - (m_1 - m_2)^2]^{1/2}}{2M}. \tag{C.3}$$

For the angular distribution of these two particles, they are isotropic and can be easily sampled by the Monte Carlo method. Their energies and momenta in the lab frame, where the initial particle has velocity $\mathbf{v} = \mathbf{p}/E$ with E and $\mathbf{p}$ denoting its energy and momentum, can then be obtained from a Lorentz transformation. The

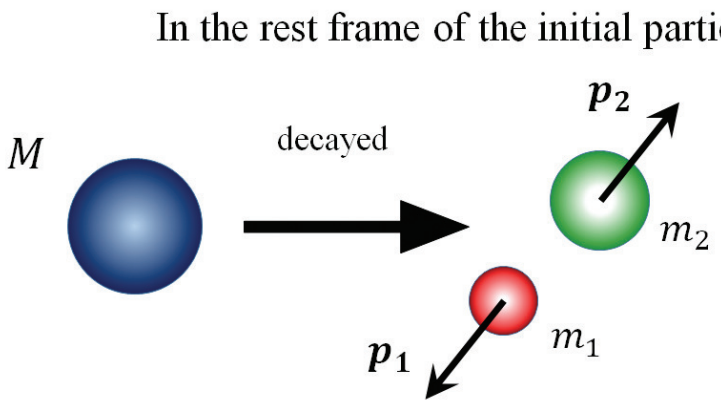

Figure C.1: The initial particle decays into two particles. In the rest frame of the initial particle, the produced particles have momenta that are same in magnitude but opposite in direction.

elements of the Lorentz transformation matrix $\mathbf{\Lambda}$ are given by

$$\Lambda^0{}_0 = \gamma, \quad \Lambda^0{}_i = -\gamma v_i = \Lambda^i{}_0, \quad \Lambda^i{}_j = \delta^i{}_j + \frac{\gamma - 1}{v^2} v_i v_j, \qquad (i,\ j = \ 1,\ 2,\ 3) \tag{C.4}$$

with $\gamma = 1/(1 - v^2)^{1/2}$.

C.2 Three-Body and Many-Body Decays

The three-body case is much more complicated. There are equations for energy-momentum conservation and, compared to the two-body case, there is an additional equation connecting the energy and momentum. We treat the three-body decay as two two-body decays. For example, as shown in Fig. C.2, the three-body decay can be regarded as a two-body decay to particle 1 and a cluster consisting of particle 2 and particle 3. The latter then decays into particle 2 and particle 3. The rest mass

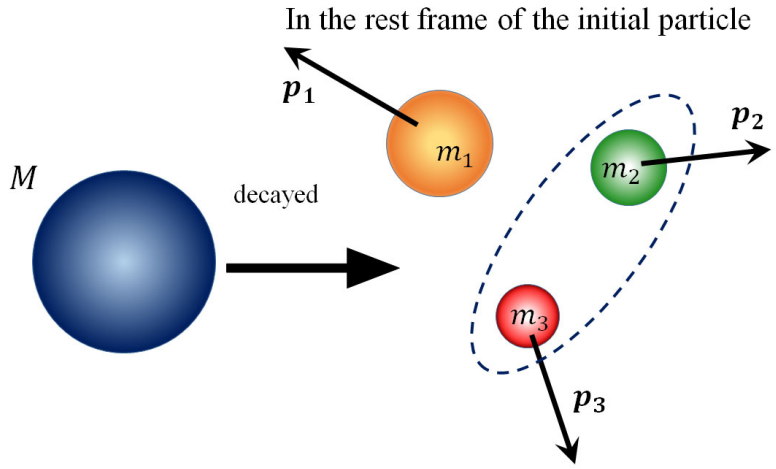

Figure C.2: The initial particle decays into three particles. The three-body decay is regarded as a two-body decay of the initial particle into particle 1 and a cluster of particle 2 and particle 3.

of the two-particle cluster or its momentum (energy) can be determined by the phase space integral

$$R_3 = \int \delta^4 \left(P - \sum_{i=1}^{3} p_i \right) \prod_{j=1}^{3} \delta(p_j^2 - m_j^2) d^4 p_j, \tag{C.5}$$

where the delta functions are due to the energy-momentum conservation. This integral can be evaluated from the convolution of the phase spaces of two consecutive two-body decays. This is shown in the following for the more general case of n-body decay.

In the more general case of n-body decay, the phase space integral is given by

$$R_n = \int \delta^4 \left(P - \sum_{i=1}^{n} p_i \right) \prod_{j=1}^{n} \delta \left(p_j^2 - m_j^2 \right) d^4 p_j, \tag{C.6}$$

Rewriting the first delta function in Eq. (C.6) in terms of the integration of two delta

functions as

$$\delta^4\left(\sum_{i=1}^{n} p_i - P\right) = \int d^4P_l\ \delta^4\left(P - P_l - \sum_{j=l+1}^{n} p_i\right)\delta^4\left(P_l - \sum_{i=1}^{l} p_i\right). \qquad \text{(C.7)}$$

we have

$$\begin{aligned} R_n &= \int\left[\delta^4\left(P - P_l - \sum_{i=l+1}^{n} p_i\right)\prod_{j=l+1}^{n}\delta(p_j^2 - m_j^2)d^4p_j\right. \\ &\times \left.\int\delta^4\left(P_l - \sum_{i=1}^{l} p_i\right)\prod_{j=1}^{l}\delta(p_j^2 - m_j^2)d^4p_j\right]d^4P_l. \end{aligned} \qquad \text{(C.8)}$$

Inserting the relation $1 = \int_0^\infty \delta(P_l^2 - M_l^2)dM_l^2$ in Eq. (C.8), we obtain

$$\begin{aligned} R_n(P, m_1, \ldots, m_n) &= \int\left[\delta^4\left(P - P_l - \sum_{i=l+1}^{n} p_i\right)\prod_{j=l+1}^{n}\delta(p_j^2 - m_j^2)\delta(P_l^2 - M_l^2)d^4p_j d^4P_l\right. \\ &\times \left.\int\delta^4\left(P_l - \sum_{i=1}^{l}\right)\prod_{j=1}^{l}\delta(p_j^2 - m_j^2)d^4p_j\right]dM_l^2, \end{aligned} \qquad \text{(C.9)}$$

which leads to the following convolution or recurrence formula

$$R_n(P, m_1, \ldots, m_n) = \int_0^\infty R_{n-l+1}(P, M_l, m_{l+1}, \ldots, m_n)R_l(P_l, m_1, \ldots, m_l)dM_l^2. \qquad \text{(C.10)}$$

From Eq. (C.10), we see that M_l^2 denotes the rest mass of the cluster of l particles. The equation decomposes the n-body decay into l-body decay plus $(n-l+1)$-body decay. When replacing l by 2 and using this formula repeatedly, an n-body decay can be decomposed into many 2-body decays as

$$R_n = \int dM_{n-1}^2 \ldots \int dM_2^2 \prod_{i=1}^{n-1} R_2(M_{i+1}, M_i, m_{i+1}), \qquad \text{(C.11)}$$

where the phase integral $R_2(M_{i+1}, M_i, m_{i+1})$ can be calculated as

$$\begin{aligned} R_2(M_{i+1}, M_i, m_{i+1}) &= \frac{\pi}{2M_{i+1}} \sqrt{M_{i+1}^2 + \left(\frac{M_i^2 - m_{i+1}^2}{M_{i+1}}\right)^2 - 2(M_{i+1}^2 + m_{i+1}^2)} \\ &= \frac{\pi \lambda^{1/2}(M_{i+1}^2, M_i^2, m_{i+1}^2)}{2M_{i+1}^2}. \end{aligned} \tag{C.12}$$

In the above, λ is defined as $\lambda(x, y, z) \equiv x^2 + y^2 + z^2 - xy - yz - zx$. Eq. (C.11) is the most important equation for solving n-body decay. The factor $R_2(M_{i+1}, M_i, m_{i+1})$ can be considered as the weight function of the rest mass of the pair of particles where M_i is the rest mass of the cluster of i particles and m_{i+1} is the mass of the $(i+1)$-th particle.

As an example, we consider the decay of a particle of mass M into three particles with masses m_1, m_2, and m_3 by using the above obtained equations. The mass M_{12} of the cluster of first two particles is restricted in a region between $m_1 + m_2$ and $M - m_3$, i.e., $m_1 + m_2 \leq M_{12} \leq M - m_3$. Eq. (C.11) for the three-body decay can then be written as

$$R_3 = \int_{m_1+m_2}^{M-m_3} dM_{12}^2 R_2(M, M_{12}, m_3) R_2(M_{12}, m_1, m_2) \tag{C.13}$$

We can generate the cluster mass M_{12} by using the Monte Carlo method. Knowing the cluster mass M_{12}, the initial particle with mass M then decays into two particles with masses M_{12} and m_3, and this is followed by the decay of the cluster of mass M_{12} into two particles with masses m_1 and m_2. As a result, we can describe the three-body decay through two consecutive two-body decays.